PHILOSOPHICAL TRANSACTIONS OF THE ROYAL SOCIETY A MATHEMATICAL, PHYSICAL & ENGINEERING SCIENCES

A Shallow Subtropical Subducting Westward Propagating Eddy (Swesty)

R. D. Pingree

Phil. Trans. R. Soc. Lond. A 1996 **354**, 979-1026
doi: 10.1098/rsta.1996.0039

A shallow subtropical subducting westward propagating eddy (Swesty)

By R. D. Pingree

Plymouth Marine Laboratory, Citadel Hill, Plymouth PL1 2PB, UK

Contents

Swesty is a shallow subtropical subducting westward propagating eddy that was observed to move across the eastern basin of the North Atlantic at a latitude near 25° N. The eddy was first detected by the movement and temperature of a drogued Argos buoy near 23° W, 26° N in February 1993. By December 1993, the drogued buoy had moved 1000 km westward to 33° W and a winter eddy survey was made from RRS Charles Darwin. The eddy was about 100 km in diameter and had a centre water mass core at a depth of 190 m with characteristic temperature 19.9 °C

Phil. Trans. R. Soc. Lond. A (1996) **354**, 979–1026
Printed in Great Britain

and salinity 37.06 psu, but was best resolved by properties related to vertical gradient structure (e.g. Brunt–Vaisala frequency, temperature perturbation structure). The eddy was particularly flat with a height-to-width aspect ratio of only *ca.* 0.14% and a vertical decay scale of *ca.* 250 m for temperature displacements. Maximum azimuthal currents were *ca.* 16 cm s^{-1} at a depth of 175 m and the eddy azimuthal transport was only 3 Sv. However, the potential vorticity in the eddy core was 1.5×10^{-11} rad ms^{-1}, comparable with other deep anticyclonic lenses and lower than background values by a factor of ten. The eddy appeared slightly elliptical with a detectable sea surface cooling (*ca.* 0.2 °C) over its centre. Three Argos buoys with drogues set at a depth of 200 m were deployed near the centre of the eddy and one buoy continued looping westward for a further *ca.* 800 km. The drogued Argos buoy results showed that the eddy moved westward at *ca.* 100 km $month^{-1}$ and about half this westward rate was attributed to self-propagation. During this *ca.* 1650 km continuously drogued journey, the eddy only slipped southward by about one degree of latitude and so was perhaps resisting the southward component of flow of the Subtropical Gyre. The buoy results suggested that the central rotation rate increased with time but the eddy became smaller. The initial rotation period of the central core was *ca.* 8 d, giving a corresponding normalized relative vorticity of −0.3. About 400 d later, the period of core rotation was *ca.* 5 d, with normalized relative vorticity of −0.5. Some of the increase in central rotation rate was attributed to subduction effects. Variance, spectra and filtered components of velocity were derived from the buoy positions. Kinetic energy levels in the eddy (*ca.* 73 cm^2 s^{-2}) were markedly elevated with respect to background levels (*ca.* 29 cm^2 s^{-2}). The core properties of the eddy indicated a winter formation near 27° N, 22° W and hydrographic sections showed that the eddy would be sinking at a rate of about 40 m a^{-1}. By the second year, the subducted water parcel, the eddy core, was sufficiently deep below the surface of the ocean to escape further effects of winter mixing.

1. Introduction

Eddies can transfer heat, salt and other passive contaminants (physical, chemical and biological) thousands of kilometres across the ocean (Kerr 1981; McDowell & Rossby 1978). Biological implications will include production, transport, reseeding and dispersal of phytoplankton, for shallow eddies penetrating or moving through the euphotic zone (Angel & Fasham 1983). While Gulf Stream rings from the western boundary of the North Atlantic Ocean are well documented, there appear to be no detailed reports of long-lived surface eddies travelling large distances from the eastern boundary of the Subtropical Gyre. This is hardly surprising since, whereas western boundary currents are particularly energetic, conditions on the eastern boundary are, by comparison, relatively stagnant, all resulting from 'western intensification' (Stommel 1958).

Deep (> 100 m) and effective droguing of satellite tracked Argos buoys has been pioneered for many years and effectively drogued Argos buoys can be used to discover and track surface eddies (Pingree 1993). One buoy, drogued for a depth of 320 m and deliberately deployed in a shallow eddy core in the Bay of Biscay, made *ca.* 60 clockwise orbits within 15 km of the eddy centre over a period of 200 d, while the eddy itself roamed some 500 km (Pingree 1994). A further buoy 3346 (drogued at a

PHILOSOPHICAL TRANSACTIONS OF THE ROYAL SOCIETY A MATHEMATICAL, PHYSICAL & ENGINEERING SCIENCES

depth of 200 m) and deployed on the same cruise (PML Cruise Report 1992) but over the Great Meteor Tablemount (*ca.* 30° N, 29° W) in March 1992, later (*ca.* 1 year) became trapped in a westward propagating eddy. This paper reports the discovery and movement of this shallow subtropical westward propagating eddy (Swesty). The eddy was relatively small with a diameter of about *ca.* 100 km and was perhaps first noted (by the movement and sea surface temperature of the drogued Argos buoy in February 1993) near the eastern boundary (*ca.* 23° W) of the Subtropical Gyre. This buoy (3346) showed the presence of the eddy continuously from about the end of April to mid-December 1993.

The realtime positions of the drogued buoy (received in the laboratory via the Argos system) meant that a hydrographic survey was possible, given a suitable ship-time opportunity. In December 1993, a hydrographic survey of physical, chemical and biological properties of the eddy was conducted from RRS Charles Darwin and three further Argos buoys, all drogued at a depth of 200 m, were deployed near the eddy centre. The original buoy and drogue, which had been in the sea for 655 d and in the eddy continuously for 241 d, was then recovered. This paper presents the results of the hydrographic survey and buoy movements which have been analysed to describe the properties and kinematics of a surface subtropical eddy (table 1). Some comparisons are made with the few known anticyclonic eddy types (i.e. with a core of water of known origin) that have been surveyed and tracked in the eastern basin of the North Atlantic (table 2).

The eddy was observed by drogued buoys continuously for about 16–17 months, and during this time it moved from 25° W (end of April 1993) almost westward (near the latitude 25° N) across the eastern basin, probably reaching a position *ca.* 41.5° W by mid-September 1994, a distance of about 1650 km, covering about one degree of longitude a month. The eddy cut across the streamlines of the Subtropical Gyre (the traditional view at least), suggesting that it was both partially self-propagating and resisting the ocean's southward movement. Overall, the results identify important aspects of mixing and movement in the ocean. They show that a discrete core of water without a distinctive water mass signature, effectively just a spinning density perturbation, of 100 km diameter and thickness of only *ca.* 150 m (*ca.* 3% of the ocean's depth, 5 km), floating near the sea surface (at a depth of 175 m), can maintain itself as an identifiable coherent structure.

2. Methods

On the basis of the track of drogued buoy 3346, showing an anticyclonic eddy moving westward along 25° N, it was decided to take the opportunity that presented itself when the embarkation port for RRS Charles Darwin Cruise 83 was Las Palmas, Gran Canaria (*ca.* 28° N) and make a survey of this eddy. On the outward leg in December 1993, hydrographic sections of temperature and salinity were derived from expendable bathythermograph (XBT) and conductivity temperature depth (CTD) stations, from a longitude 16.5° W to 34° W near the latitude 25.5° N, along the route taken earlier by the eddy to its late December position (figure 2).

The hydrographic observations of the eddy survey included 35 XBT profiles (largely T5s, with profiles from the surface to 1800 m), 14 CTD profiles (from the surface to 2000–3000 dbar) and four SeaSoar runs into the eddy centre, all conducted within a *ca.* 4 d period (19–22 December 1993, figure 3). The SeaSoar is a towed undulating CTD allowing underway profiling to depths of 400 m at a speed of *ca.* 7 kt. The SeaSoar

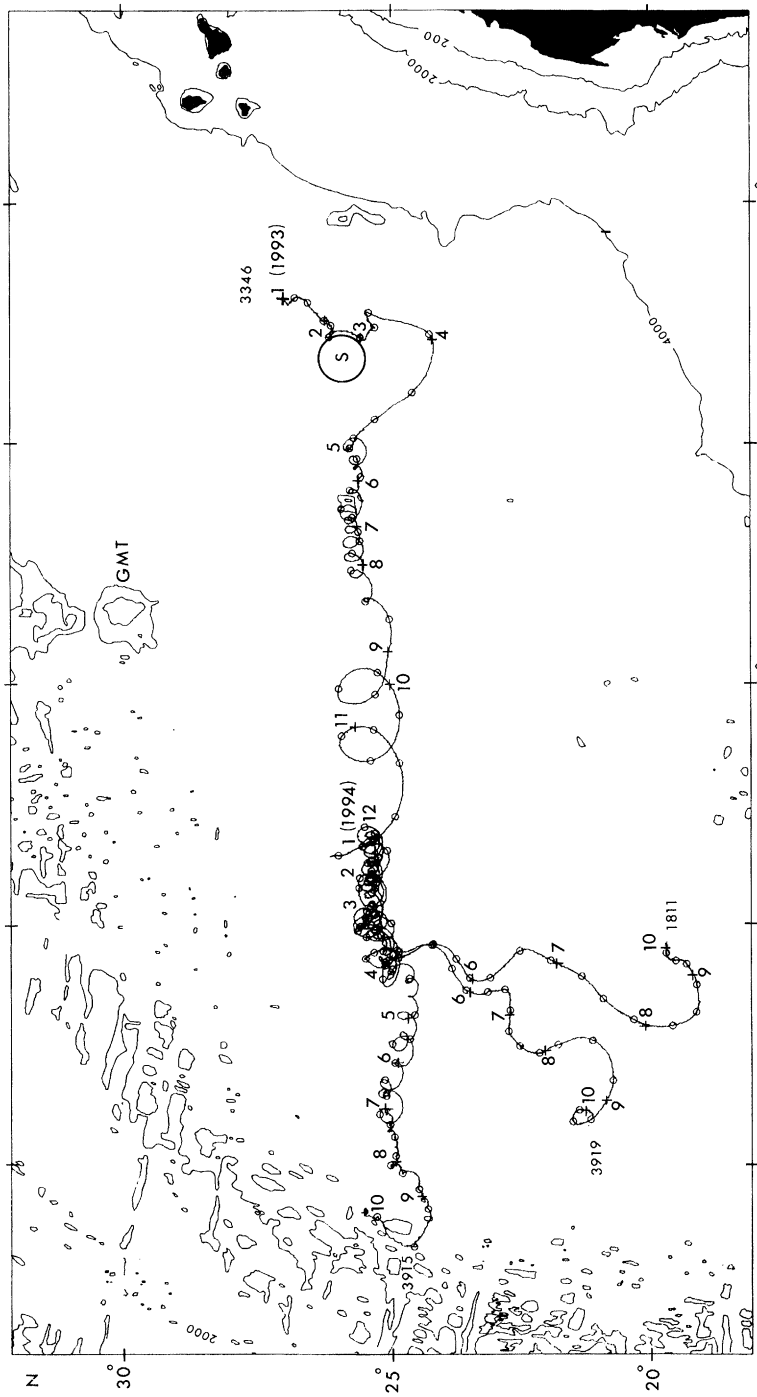

Figure 1. Raw data tracks of Argos buoys 3346, 1811, 3919 and 3915, all drogued at a depth of 200 m, covering the period from yearday 1 (1993) to yearday 643 (5 October 1994) showing movement of Swesty. Buoy 3346 was originally deployed over the Great Meteor Tablemount (GMT) and was in the eddy continuously for *ca.* 241 d. Buoys 1811, 3915 and 3919 were deployed during the December 1993 eddy survey when 3346 was recovered. 1811 and 3919 came out of the eddy after about 125 d; 3915 lost its drogue on about the 12 September 1994. Months (1993 and 1994) are indicated by numbers 1–12 and the mean eddy translation is about 1 degree of longitude per month (*ca.* 100 km month^{-1}); circles are at 10 d intervals. At a depth of 200 m, the eddy carries with it water to a radius of *ca.* 50 km and a circle marked S of radius 50 km is shown at a suggested initial position for the eddy in February 1993. Water depth contours are 200 m, 2000 m and 4000 m; the coast of Africa is to the east and the Mid Atlantic Ridge is to the west.

Table 1. *Characteristics of Swesty*

property (units)	core CTD 14	external CTDs 7/20
depth (m)	190	190
salinity (psu)	37.06	36.71
temperature (°C)	19.9	18.5
oxygen (ml l^{-1})	4.8	4.5
nitrate (μM)	0.5	1.5
silicate (μM)	0.8	1.0
density σ_t (kg m^{-3})	26.36	26.44
Brunt–Vaisala frequency (cph)	1.0	3.0
aspect ratio (%)	0.14	—
rotation period (d)[a]	8	—
vorticity ζ/f	−0.3	0.0
absolute vorticity $f+\zeta$ ($\times 10^{-4}$ s^{-1})	0.43	0.615
potential vorticity ($\times 10^{-11}$ rad ms^{-1})	1.5	18
mean west speed (cm s^{-1})	3.7	1.5
south–west aspect ratio (%)	6	—
NS–EW variance ratio (%)[b]	95	—

[a]Local dynamic properties refer to the time of the eddy survey December 1993.
[b]Mean of all buoys in the eddy.

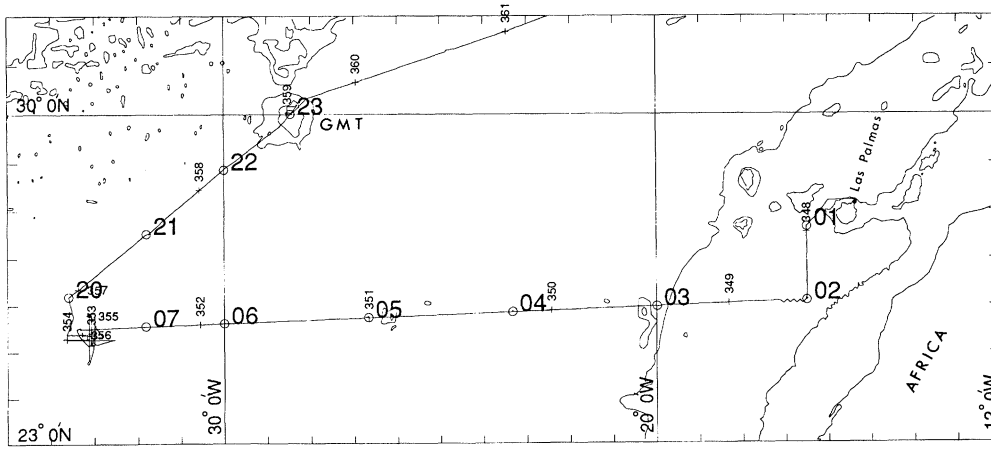

Figure 2. Map showing the track of RRS Charles Darwin from Las Palmas, Gran Canaria (yearday 347, 1993) along the route taken by Swesty to the eddy survey region (yeardays 352–357). Crosses, yearday; circles, CTD station positions (1–7 and 20–23). CTDs 07 and 20 were at a radial distance of about *ca.* 100 km from the eddy centre and the ship left the eddy survey region via CTD 20, passing the Great Meteor Tablemount (GMT) on yearday 359.

deployment was continuous with a down and up cycle of 15 min for *ca.* 30 h, effectively

Table 2. *Comparison of characteristics with other anticyclonic lenses*

	Swesty Flatty	Meddy Bobby	Meddy Sharon	Meddy Pinball	Smeddy Tagus	Swoddy F90a
water mass depth (m)	190	1300	1200	685[a]	700	150
salinity (psu)	37.06	36.53	36.56[b]	36.40	36.48	35.74
temperature (°C)	19.9	12.1		13.1	13.6	13.0
density σ_t (kg m^{-3})	26.36	27.76		27.46	27.43	26.97
oxygen (ml l^{-1})	4.8	4.3		4.5	4.7	
nitrate (μM)	0.5	16		6	12	
silicate (μM)	0.8	12		5	7	
dynamic core depth[c] (m)	200	1200	1050	700	700	150
Brunt–Vaisala frequency (cph)	1.0	1.0	1.0	1.1	1.2	0.2
rotation period (d)	8	4	6	2.5	4	3
central vorticity $-\zeta/f$	0.3[d]	0.5	0.4	0.65	0.45	0.5
potential vorticity (10^{-11} rad ms^{-1})	1.5	1.2	3	1.2	2.1	0.07
aspect ratio (%)	0.14	1.8	1.0	2.0	1.6	0.5
azimuthal current maximum (cm s^{-1})	16	30	25	30	20	30
at a radius in km	30	22	25	35	12	30
azimuthal transport (Sv)	3	10		13	4	8
to a radius in km	50	50		50	50	70
net observed travel (km)	1650	50	1100	300	150	500
over period (months)	16.5	0.5	24	7	1	10

[a]Upper core values.
[b]Properties refer to first survey (Oct 84).
[c]Estimate based on the centre depth of the broad potential vorticity minimum.
[d]At the time of the eddy survey.

providing another *ca.* 220 CTD dips. The CTD was equipped with an oxygen sensor and the oxygen profiles were calibrated with discrete water samples drawn from the rosette multisampler, further samples were taken for analyses of nitrate, phosphate and silicate (see PML Cruise Report (1994) for more details). Light transmission (for beam attenuation coefficient) and chlorophyll 'a' fluorescence profiles were also made but as this was not the productive season these properties only showed a small (but nevertheless just evident) influence of eddy structure on primary production and are not presented in detail.

The eddy current structure was determined indirectly using the gradient or geostrophic relation and measured directly with the ship's hull-mounted RDI ADCP transducers (153 kHz, profiles to 300 m) and also by position fixing (Argos system) of buoy 3346 and the three further deliberately deployed drogued buoys, 1811, 3915 and 3919. One ALACE float (Davis *et al.* 1992) was also deployed but failed to transmit subsequently.

The initial XBT–CTD–SeaSoar survey was aimed at determining the eddy structure, centre and the mid-depth of the core. Drogues were set to a depth of 200 m. This

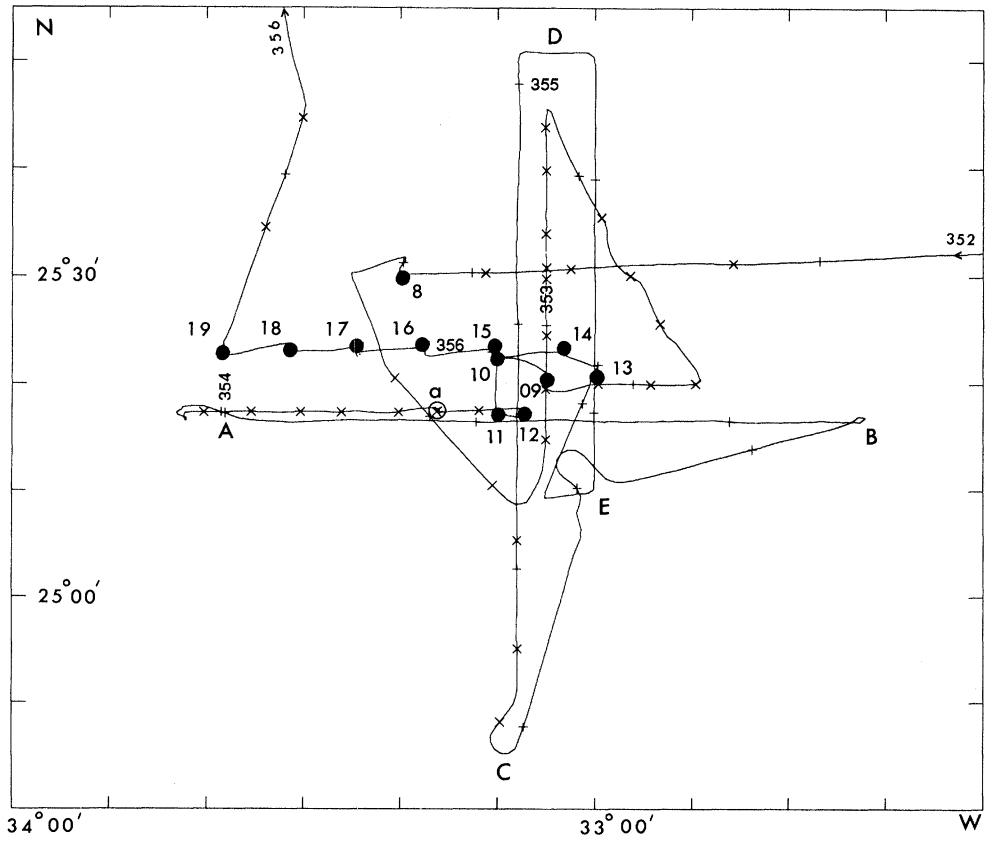

Figure 3. Track of RRS Charles Darwin from yearday 352 to 356, 1993. Vertical crosses on track mark 3 h intervals and yearday is annotated. CTD station positions (8–19) shown by solid dots and XBTs station positions (41–74, not numbered) indicated by diagonal crosses. ABCDE is a run with the SeaSoar deployed, allowing continuous profiling to *ca.* 400 m. The deployment position of Argos buoy 1811 was at CTD 12 (yearday 353), buoy 3915 was deployed at the position indicated by a circle labelled 'a' (also XBT 64, yearday 353) and buoy 3919 was deployed at CTD 14 on yearday 355, when the eddy centre was 3 km west of CTD 14.

drogue depth was actually just below the centre of the eddy core, which varied from *ca.* 150 to 200 m, depending on which parameter was used to estimate a centre depth. The 200 m level was chosen so that the results would be directly comparable with those already derived from the movement of buoy 3346. Buoys 1811 and 3915 were deployed on yearday 353. Buoy 3919 was deployed on yearday 355 in a position believed at the time to be the eddy centre, where CTD 14 was also conducted. Buoy 3919 looped initially at a radius of *ca.* 8 km, showing that the eddy centre was in fact already about 3 km west of the position of CTD 14 when this station was conducted. At the 200 m level, vertical shears were small during the survey period and, as a first approximation, the drogued buoy movements are considered as representing water movement at a depth which corresponds to the centre depth of the eddy core (but see later § 4 *c*).

CTDs 14–19, with stations every 12 km, were used to derive accurate vertical sections of water properties through the eddy along a 60 km radial line stretching westward (at 25.38° N (figure 3), and along which the eddy centre subsequently passed)

from CTD 14. For comparison, water properties at CTDs 7 and 20 at a radius of *ca.* 100 km (figure 2) were used to characterize the local background water properties. Contoured sections have been prepared with radial distance measured from CTD 14, the most central CTD station, and a correction (amounting to a 2 km compression of the section) for the translation of the eddy during the measurements has been applied.

Plan views of the eddy structure at different depths were derived from XBT, CTD and SeaSoar measurements with respect to a moving centre (*ca.* 3 km d^{-1} westward) by taking into account the time of each measurement and making a displacement correction to compensate for the westward movement of the eddy during the survey. Since the survey was relatively rapid (*ca.* 4 d), the position corrections only ranged from 0 to *ca.* 12 km.

No clear infrared images of this eddy have yet been obtained, the main difficulty being that its southern location is beyond the range of the data received routinely via the satellite receiving station at the University of Dundee.

XBT/ADCP data are derived against depth in m, whereas CTD data are profiled against pressure in dbar. Depths are referred to by both metres and dbars, the numerical difference being about two for conditions at 200 m–200 dbar. CTD pressures and XBT depths (Narayanan & Lilly 1993) were calibrated and, where XBT and CTD temperature data are used together, a conversion correction has been applied. Yeardays, used to denote time, start 1 January 1993, since the eddy was first noted in 1993; 1 January 1994 is yearday 366; buoy 3915 (last buoy in the eddy) lost its drogue on yearday *ca.* 620 (12 Sept 1994).

The paper first discusses the hydrographic structure determined during the RRS Charles Darwin survey and this is followed by results showing the current structure of the eddy. Significance of the westward movement, eddy origin, eddy decay scales and small-scale mixing follow. The final part of the paper examines the kinetic energy structure and, by filtering in the frequency domain, separates eddy and inertial energy bands and discusses drogue loss.

3. Results: hydrographic structure

(*a*) *Temperature, salinity and density sections along* 25.5° N

CTDs 2–7 and 20 (figure 2) were used to derive zonal sections of temperature, salinity and density across the eastern Subtropical Gyre from 16° W to 34° W (figure 4). Although CTD profiles were to 2000 m, only the upper 500 m of the section is shown as gradients were relatively small below 1000 m. Of significance with respect to the core characteristics of the eddy (see § 6) are temperatures near 20 °C, which only occur below the seasonal thermocline and to the east of *ca.* 20° W in mid-December. In contrast, salinity values above 37 psu are confined to the surface mixed layer (*ca.* 100 m deep) to the west of 19° W. Isopycnal surfaces slope downward to the west and southward geostrophic flows (with a reference level of 2000 dbar) were typically 0.5 cm s^{-1} at a depth of 800 m, 1 cm s^{-1} at 500 m and 2 cm s^{-1} at the sea surface, west of 20° W. The southward transport between 20° W and 34° W was determined as 16.4 Sv. To the east of 20° W, the deep isopycnals sloped downward to the east and the geostrophic flow was northward with transport *ca.* 6.7 Sv.

The overall values from this section (§ 3 *a*) are used to appraise the eddy results in § 5 and § 6. Between CTD 2 and CTD 7 (which was about 100 km from the eddy centre) there were 26 temperature profiles, including the XBT profiles, with a station every

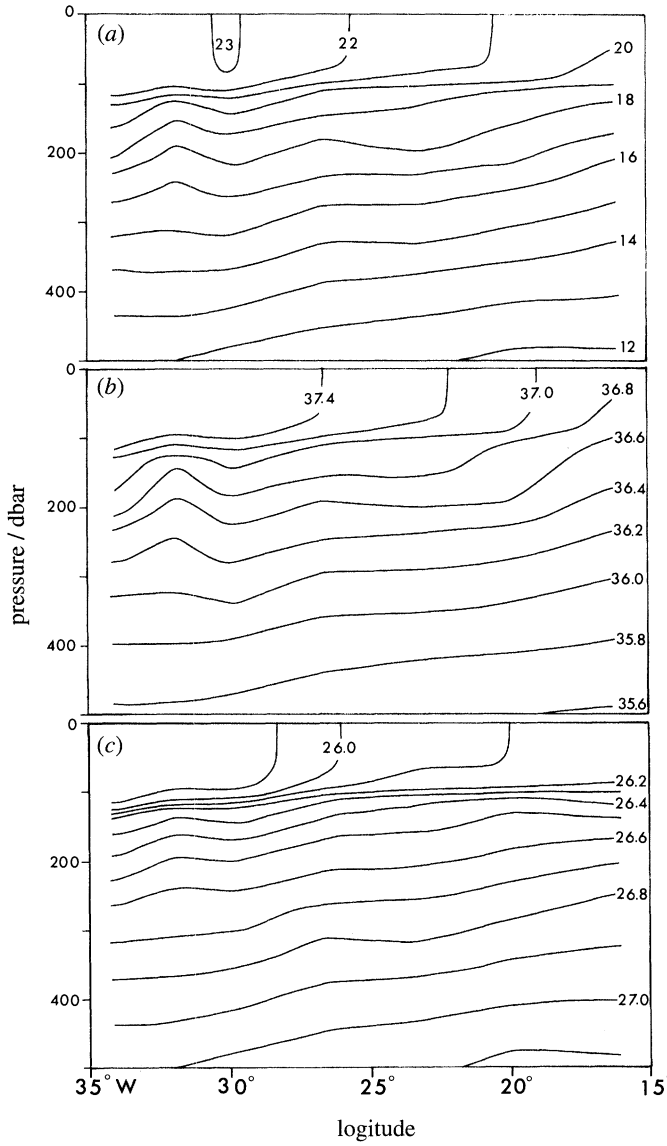

Figure 4. Vertical sections of pressure (dbar) against longitude (° W) showing contours of (*a*) temperature (°C), (*b*) salinity (psu) and (*c*) σ_0 (kg m^{-3}) from *ca.* 16° W to 34° W along the route (*ca.* 25.5° N, see figures 1 and 2) taken by the eddy, derived from CTD stations 2–7 and 20. Note surface salinities > 37 psu are west of 19° W and winter mixing (December 1993) is bringing surface temperatures down to *ca.* < 20 °C in the east of the section.

ca. 55 km. No eddies were found on the outward route to CTD 7 and perhaps would not be expected if winter mixing (i.e. after December) was necessary for production (see § 6).

(*b*) *Temperature profiles through the eddy, T–S plots*

Temperature profiles from CTD stations (8–19) are used to describe the structure and the water properties of the eddy. CTD temperature profiles 13–20, ranked radially

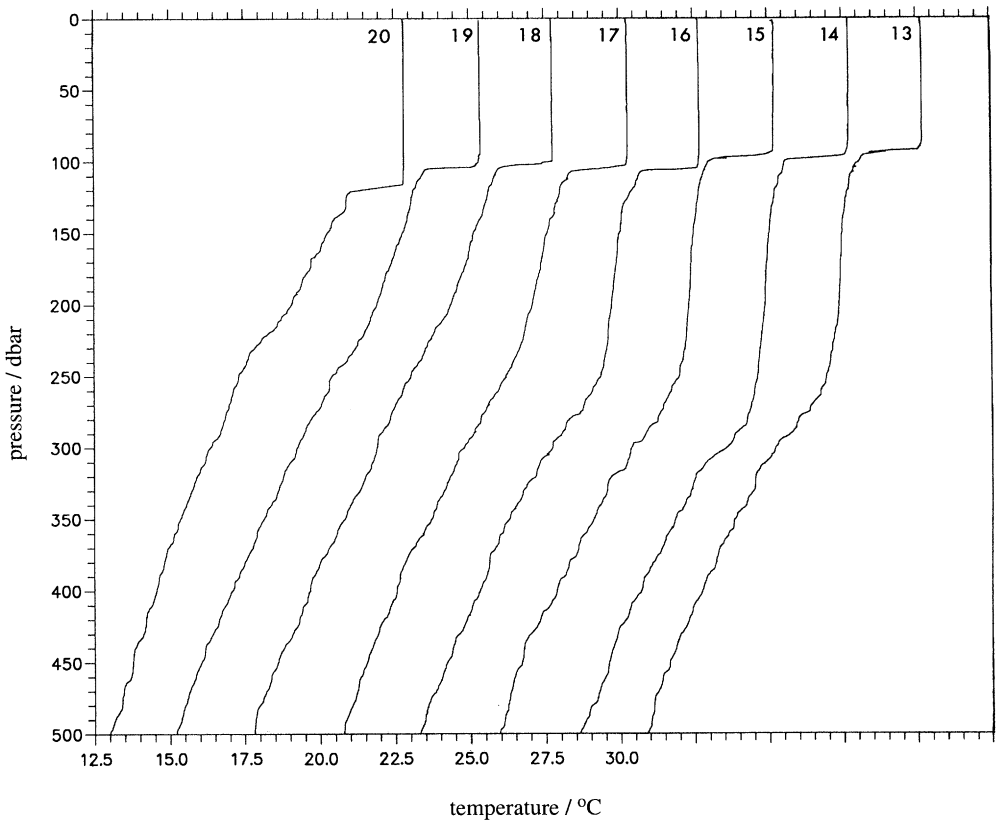

Figure 5. Temperature profiles from 0–500 dbar for CTDs 13–20 showing maximum core development (*ca.* 150 m thick) at CTD 14. Temperature scale is for CTD 20 and each profile is displaced by 2.5 °C.

from east to west, show the presence of the shallow lens of water just below the eroding seasonal thermocline clearly (figure 5). The most homogeneous region of core water occurs at a depth of 190 m at CTD 14, where the salinity was *ca.* 37.06 psu.

The eddy core temperature (19.9 °C), salinity (37.06 psu) and density (σ_t = 26.36 kg m^{-3}) characteristics at 190 m (table 1) are not very conspicuous on a T–S plot (figure 6) as local water with similar temperature and salinity properties occurs in a narrower region near the base of the seasonal thermocline. It is perhaps more remarkable how similar the T, S properties are at the different CTD stations, in the upper *ca.* 500 m (i.e. figure 6) and especially below *ca.* 200 m, bearing in mind that CTD 2 is about 1700 km east of CTD 20. Although not really distinctive on a T–S curve, the characteristic core properties are important in establishing an origin for the eddy. These properties outcrop at the sea surface in winter and the values (also oxygen, see § 3 *e*), together with the measured eddy translation, have been used to deduce a likely position for the eddy formation (see § 6). Overall, the temperature and salinity changes are well correlated but have opposing effects on density changes with temperature dominating changes by an overall ratio of about 1.8:1.

(*c*) *CTD and SeaSoar temperature and salinity sections*

Temperature and salinity sections were contoured from CTDs 14–19 to give a 60 km radial cut of the eddy core properties (figure 7). The temperature section shows a

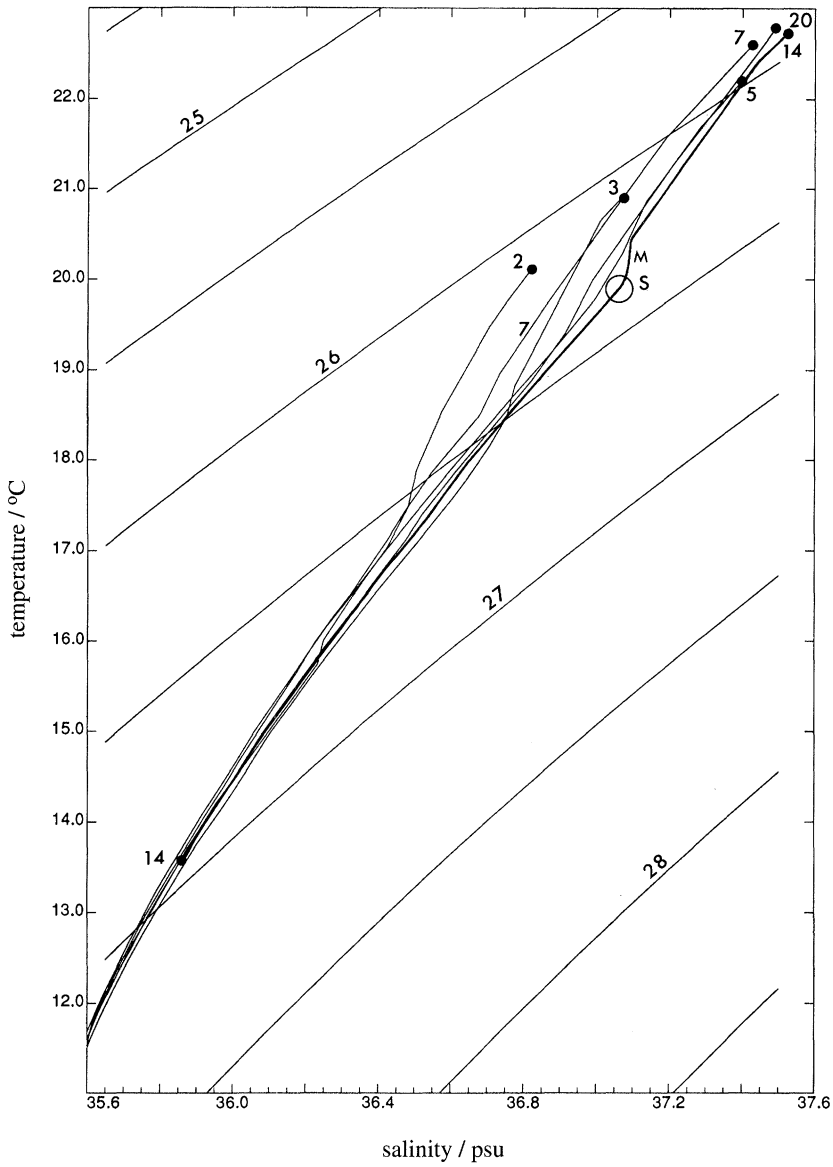

Figure 6. Temperature (°C) and salinity (psu), T–S curves of CTDs 2, 3, 5, 7, 14 and 20. Mixed layer values (dots) generally extend downwards for *ca.* 50–100 m. CTD 14 (bolder line) is through the eddy centre and the circle (marked 'S' (Swesty)) represents about 50 m of the eddy core centred near a depth of 190 m. The region M above the central core S is thought to be 'modified' core water (see text for details). The σ_t 26.5 kg m^{-3} cuts the curves in the depth range *ca.* 130–230 m (see figure 4) and the 27.0 line in the range *ca.* 400–500 m, except at CTD 14, where the lower dot is at a depth of 505 m, as the isopycnals are depressed below a depth of *ca.* 175 m at this station. The T–S curve is particularly well defined for temperatures below about 17 °C. Changes in properties horizontally are small; CTD 2 is 1600 km east of CTD 14, CTDs 7 and 20 are 100 km from the eddy centre.

thickening of the 19–20 °C isotherms near CTD 14 and the 19.9 °C isotherm characterizes the central core temperature at a depth of 190 m. The doming of the seasonal

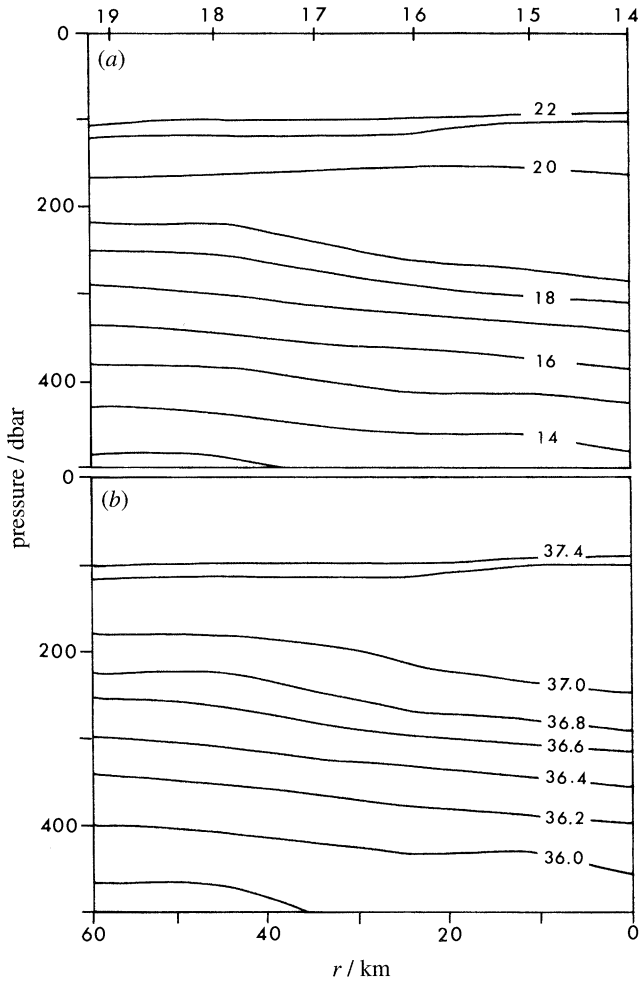

Figure 7. (*a*) Vertical temperature (°C) section of pressure (dbar) against distance (r) measured radially in km from CTD 14 showing eddy core temperature (*ca.* 19.9 °C at a pressure of 190 dbar, CTD14). (*b*) Corresponding vertical section of salinity (psu) showing salinity core (37.06 psu at 19.9 °C, CTD 14). CTD stations indicated. Note the absence of a distinct water mass core.

thermocline over the eddy core means that this eddy, like other near-surface (i.e. core centre within the top 0.7 km of the water column (see Pingree 1995)) anticyclonic lenses could have an infrared remote-sensing sea-surface signature (see § 3 *f*).

The salinity section (figure 7*b*) shows the same thickening of core water but the salinity core is somewhat shallower with a central (maximum separation between contours) isohaline (*ca.* 37.075 psu) at a depth of about 145 m. The vertical scale of the core structure is about 200 m (estimated approximately on a basis of a notable change of vertical gradient at the eddy centre) and the horizontal extent is about *ca.* 60 km (this is also about the maximum radius of the water travelling with the eddy), giving the structure a height-to-width scale or aspect ratio of 0.2%. This is perhaps an overestimate since the isohalines confining the core have a far field thickness or separation of *ca.* 80 m (for 0.4 psu difference, say), thus reducing the value to *ca.* 0.1%. The near surface eddy is therefore particularly flat in comparison with other

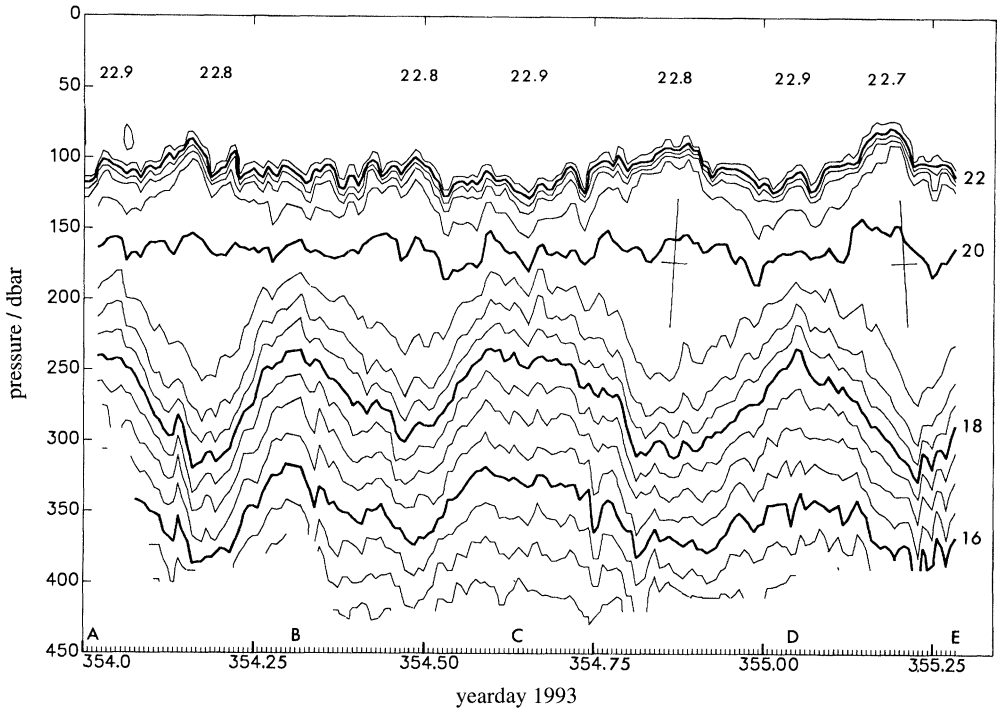

Figure 8. SeaSoar pressure (dbar) against time (yearday 1993) sections of isotherms (°C) showing cuts through the eddy. ABCDE indicated (see figure 3). The lens is less thick between B and C as the centre was only approached, not crossed. Note opposite tilts (slope *ca.* 1E−4) in the lower regions of the last two cells (see text). Tick marks are at 10 min intervals and a vertical profile was obtained every 7.5 min.

deep anticyclonic lenses (cf. meddies *ca.* 1–2%, table 2), and this particular Swesty became known as 'Flatty'.

SeaSoar sections show the near surface lens most clearly. The sections are presented against time and with steady SeaSoar towing, at 7.75 kt, 1 h is equivalent to *ca.* 14 km (see also figure 3). 40 m peak-to-trough oscillations of the thermocline (mean depth 110 m) matching in antiphase *ca.* 80 m oscillations of the 18 °C isotherm (mean depth 270 m) reveal the eddy core (figure 8).

A near-level isotherm (*ca.* 20 °C, or rather 19.95 °C) occurs at a depth of about 170 m. The maximum separation between isotherms in the eddy core occurs at a depth near 190 m, where the temperature is 19.9 °C. So a central core isotherm is slightly depressed in the eddy core with respect to its far-field level. Since changes of temperature largely control density changes, corresponding SeaSoar isopycnal sections (not shown) look similar to figure 8. A depression of the central isopycnal in the eddy core with respect to the far field has been observed in other anticyclonic lenses (see, for example, Pingree & Le Cann 1993*a*), and is thought to reflect the general decrease of static stability with depth (i.e. the tendency for a hydrostatic balance and, also in this case, the eddy core is near the sea surface and restricted by this boundary as well as the seasonal thermocline).

The maximum slope of the 18 °C isotherm is only about 0.16% and this fairly uniform gradient is maintained for a large proportion of the crossing radius. If a

contribution is added from the upper layer to 0.16%, then the eddy aspect ratio is about 0.2%, rather larger than before as it is based on maximum slope.

The near homogeneous core and surrounding density structure imply a geostrophic anticyclonic flow of core properties (see § 4). Westward movement of the core (which might be interpreted as revealing the beta effect, see § 5 *a*) is interpreted from the slope of the deeper (400 dbar) isotherms on the south–north leg between C and D, where the isotherms beneath the near-level central core isotherm (20 °C) are shallower at C than at D for the same radial distance from the eddy centre. Note also the opposite tilt tendencies of the lower core axis for the last two sections of figure 8. Background levels are thought to tilt downward to the west at the 400 dbar level (Levitus 1982; Armi & Stommel 1983; see also figure 4). An adjustment of the south-to-north isotherms (isopycnals) to the background levels would imply a weak eastward return flow exterior to the eddy, where the local eastward transport is comparable to the westward transport of the water moving with the eddy core (i.e. the eddy core moving through the ocean). At a radius of 50 km with respect to the centre of the eddy, the mean isopycnal slope between 200 and 500 dbar was estimated as *ca.* 1.5×10^{-4}. An estimate for the westward flow in the eddy core (at the *ca.* 200 dbar level) is then 1.5 cm s^{-1}. The ocean itself is moving westward (*ca.* 1.5 cm s^{-1}, see § 5 *a*) at this level, giving a total westward speed of *ca.* 3 cm s^{-1} for the eddy. At higher levels *ca.* 170 m (*ca.* 20 °C), the mean background levels generally tilt upwards to the north (beta spiral dynamics, Armi & Stommel 1983), so, relative to background, the 20 °C isotherm might still tilt downward. Thus, it seems likely that the thermocline and the mixed layer are moving westward with the eddy.

A maximum sea surface cooling of about 0.25 °C was detectable near the centre of the eddy (see also § 3 *f*) and this is quite remarkable as, in this case, it cannot be simply due to the lifting of the isotherms (isopycnals) over the eddy core. Winter mixing has created a mixed layer in which the water properties are uniform over a vertical extent of *ca.* 100 m. In this mixed layer, the temperature was isothermal to the order of a thousandth of °C (figure 5) and so the cooling might imply a vertical circulation, with upward flow at the top of the seasonal thermocline and horizontal divergence above and convergence below. It is possible that the tip of the rotating core, pressed up from below and under enhanced internal oscillations of the core, thinned (or eroded) the seasonal thermocline from below allowing periodic mixing and heat transfer, essentially resulting in a 'leak'.

Alternative hypotheses, or additional processes enhancing the above, are that the eddy has carried with it a cooler non-local surface wind-mixed layer or that heat loss at the sea surface has cooled the shallower mixed layer over the core relatively more than the deeper mixed layer in the surrounding waters. A sea surface cooling has been noted over anticyclonic lenses at other times of the year (see, for example, Pingree & Le Cann 1992*a*).

(*d*) *Isopycnal surfaces and static stability*

σ_t (surface reference pressure, *in situ* temperature), or σ_0 (surface reference pressure, potential temperature), is adequate to represent the isopycnal displacements for a surface eddy, particularly for an eddy without a distinctive water mass signal, where changes of temperature and salinity along an isopycnal surface are small (if they are not, then a relevant reference pressure must be adopted). σ_0 contoured from CTDs 14–19 showed the level isopycnal at *ca.* 175 m (figure 9*a*). The level isopycnal is dynamically significant (i.e. the level of maximum tangential geostrophic currents,

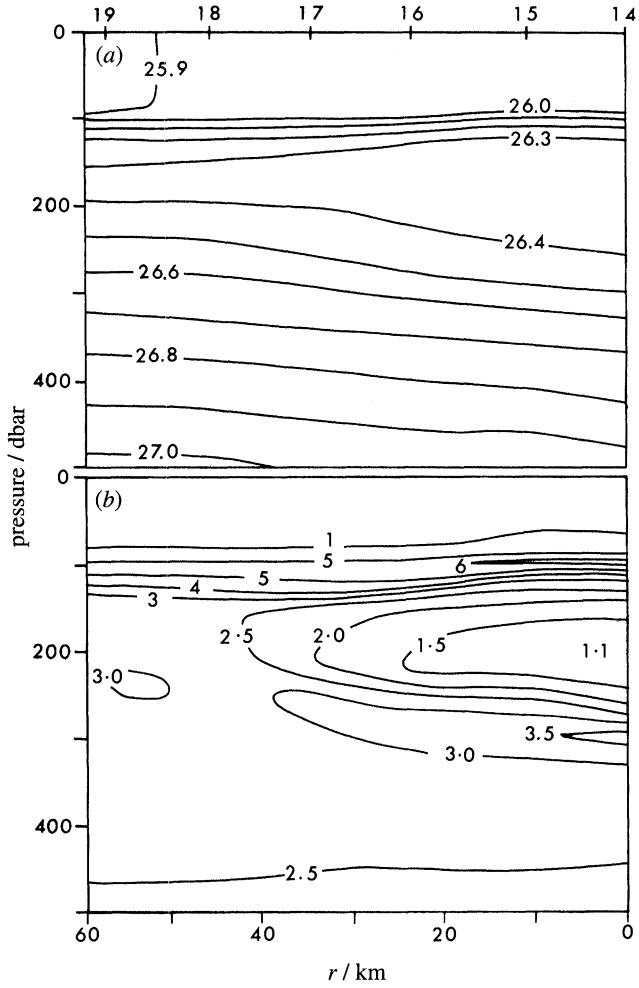

Figure 9. Vertical sections with pressure (dbar) against distance (r) measured radially in km from CTD 14 of (*a*) σ_0 showing isopycnal surfaces increasing at intervals of 0.1 kg m^{-3}. (*b*) Brunt–Vaisala frequency (cph) showing minimum of *ca.* 1.1 cph at 200 dbar. CTD stations indicated.

see § 4 *a*) and also shows that the centre of the eddy core is just warmer (*ca.* 0.2 °C) and saltier (*ca.* 0.06 psu, see also figure 6) than at a radius of *ca.* 60 km when changes are considered along a fixed isopycnal surface; local horizontal changes of temperature and salinity at the central core depth (*ca.* 190 m) are substantially larger (see table 1, figure 4). The $\sigma_0 = 26.365$ kg m^{-3} isopycnal at 190 m characterizes the eddy core and the separation between adjacent isopycnals in the core is stretched by a factor *ca.* 5 with respect to far-field values at a radius of 60 km.

The outward section (figure 4) shows that the $\sigma_0 = 26.37$ kg m^{-3} isopycnal has descended from a depth of *ca.* 115 m at 23° W to *ca.* 165 m at 34° W along the track of the eddy. This isopycnal surface will continue to descend westward (to balance the southward Sverdrup transport), reaching values of about 185 m over the centre of the Mid-Atlantic Ridge (*ca.* 45° N) (historical data, Levitus 1982). The density sections therefore show that the eddy core was probably sinking slowly (*ca.* 40 m a^{-1})

as it tracked westward and, at a *ca.* 40° W position, would be about *ca.* 50 m deeper than at *ca.* 25° W. As the eddy subducts, the sea surface cooling signature would be expected to diminish.

The T–S relationship is well defined, so maximum isopycnal displacements, like the isotherm displacements, are about 80 m at a depth of *ca.* 270 m and are effectively absent or lost in variability at 800 m, a depth which can be considered as the maximum depth to which the dynamic structure penetrates. As expected, isopycnal displacements are significant above the eddy core (*ca.* 40 m, in the seasonal thermocline (*ca.* 110 m) but not sufficient to cancel the geostrophic tangential flows which extend to the sea surface (see § 4 *a*).

Density (and salinity) surfaces were also derived from the SeaSoar temperature, salinity and pressure data, and were, as expected, similar to the isotherms. The salinity lens (near-level isohaline *ca.* 155 m, maximum separation between isohalines at *ca.* 145 m) was shallower than the temperature lens (maximum separation between isotherms at *ca.* 190 m), but this salinity difference had only a small effect on the density distribution and the maximum separation between isopycnals occurred near a depth of 195 m (i.e. core depth for minimum Brunt–Vaisala frequency), with a near-level isopycnal at 175 m. The maximum separation between isohalines (near *ca.* 145 m depth in the eddy core) also meant that there was a region just below the seasonal thermocline (*ca.* 120 m) where the centre of the top of the core was fresher (*ca.* 0.05 psu) than at a larger radial distance (*ca.* 60 km) along a fixed isopycnal.

Some differences in salinity profiles with respect to temperature profiles in the eddy core may have occurred as the seasonal thermocline developed, modifying the upper core properties. The region marked M on the T–S curve of CTD 14 (figure 6) might represent a *ca.* 0.4 °C warming of the upper core as the thermocline was established. Loss of warmer surface water from the eddy might occur as the thermocline develops, and the surface density contrast increases with respect to the unmodified core water below.

Static stability structure is conveniently examined in terms of the Brunt–Vaisala frequency N, defined as

$$N^2(p) = -\frac{g}{\rho}\left(\frac{\partial \rho}{\partial z}\right)_p, \tag{3.1}$$

where g is the acceleration due to gravity, ρ is the density and changes with respect to z are referred to the pressure p at the depth of interest.

To reduce noise, (3.1) must be approximated by its finite-difference form. CTD profile values were averaged into 20 m intervals and a vertical difference value, Δz, of *ca.* 20 m was used and found sufficient to allow continuity of structure from one CTD profile to another. The eddy centre is, as expected, associated with a region of minimum stability in the core, at a depth of 200 m (figure 9*b*), and the minimum value *ca.* 1.1 cph is comparable with that found for other anticyclonic eddies (table 2). Below, at a depth of 300 m, there exists a maximum value of N with corresponding frequency *ca.* 3.8 cph. This region is assumed to represent the lower boundary of the water comprising the subducted eddy core. The maximum above (in the seasonal thermocline), with a value of *ca.* 7 cph at a depth of 100 m, represents the upper boundary or upper influence of the eddy core, giving the core a thickness of about 200 m between these two anomaly maxima.

The squeezing of the thermocline isopycnals (isotherms) by the eddy core can been seen in the SeaSoar temperature section, see isotherms 20.5 and 21 °C (figure 8). The

PHILOSOPHICAL TRANSACTIONS OF THE ROYAL SOCIETY A MATHEMATICAL, PHYSICAL & ENGINEERING SCIENCES

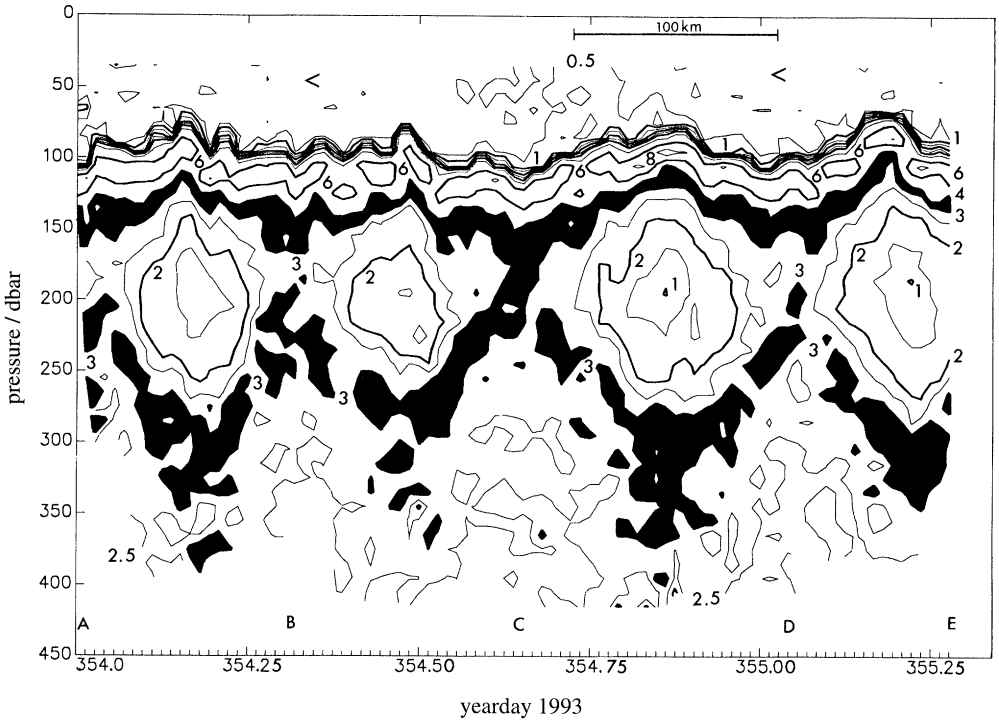

Figure 10. SeaSoar section of Brunt–Vaisala frequency (cph) corresponding to figure 8 (using a vertical interval of 10 m for calculating the density gradient) showing eddy density gradient structure. Contours at 0.5, 1.0, 1.5, 2.0, 2.5, 3, 4, 6, 8 cph. Mixed layer values < 0.5 cph, thermocline *ca.* 6 cph and shading between 3 and 4 cph contours highlights the lens with minimum values of 1.0 cph near 195 dbar on the last two sections. Tick marks are at 20 min intervals and include a down and up profile (*ca.* 15 min). 100 km scale shown.

lower maximum is evident by the squeezing and stretching between the 16 and 18 °C isotherms. The core region of minimum $N \sim 2.5$ cph, between the two maxima, is about 140 m vertical extent, and this minimum extends to a radius of about 42 km giving an aspect ratio similar to that found for the other properties. This structure is seen repeatedly in the actual SeaSoar section of Brunt–Vaisala frequency (figure 10). The eddy centre based on minimum N is at *ca.* 200 m, with values just reaching 1.0 cph at *ca.* 195 m. The third cell (figure 10), with a near central crossing of the eddy, gives a clear visualization of the eddy shape with an aspect ratio of 0.14% based on the 3 cph contour, and this value has been chosen to characterize the eddy (table 1), though it is clear that internally (1.5 cph contour) the aspect ratio increases to *ca.* 0.2%.

(*e*) *Passive tracers*

(i) *Inorganic nutrients*

A nitrate section was contoured along the radial section containing CTDs 14–19. In addition, samples drawn at CTDs 8–11, 13 were used with a correction for radial distance based on a moving eddy centre. Contours extend beyond CTD 19 using values at CTDs 7 and 20. The nitrate contours (figure 11*a*) show a structure similar to salinity. Surface values are less than 0.05 μM and the eddy core can be seen as

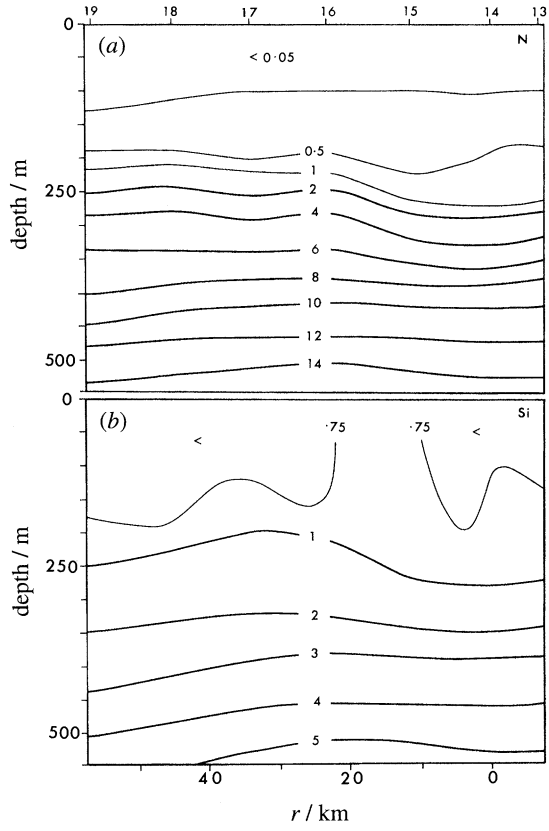

Figure 11. Vertical sections, with depth (m) against radial distance r (km) from CTD 14, of (a) nitrate (μM), (b) silicate (μM). CTD stations marked.

a deepening of the 1 μM contour. The low nitrate lens, values between 0.05–1 μM, extends horizontally to a radius of about *ca.* 50 km and the separation between these contours is stretched vertically by about 100 m near the eddy centre with respect to far-field conditions, giving an aspect ratio for the nitrate structure of *ca.* 0.1%. By contrast, the silicate contours show a less well-resolved feature, but the lower central part of the eddy core is still clearly identifiable by the 1 μM contour (figure 11*b*). Towards the sea surface, the nitrate levels are reduced relatively more than the silicate values so the Redfield ratio (Si/N) increases markedly near the base of the mixed layer (figure 12*a*).

(ii) *Oxygen*

The corresponding oxygen section (figure 12*b*) shows a deepening of the 4.8 ml l^{-1} contour from *ca.* 150 m to *ca.* 250 m associated with the eddy core. The small (*ca.* 0.2 ml l^{-1}) but general increase in oxygen concentration in the core region (*ca.* 200 m depth) also indicates a surface origin for the core water.

The upper core of the eddy is a region of increased oxygen concentration (as indicated by the 5.0 ml l^{-1} contour near 120 m) and elevated values tend to extend along the base of the mixed layer. The December levels of chlorophyll 'a' fluorescence and beam attenuation coefficient were all uniformly low and showed little structure in the profiles except at the base of the seasonal thermocline where fluorescence levels

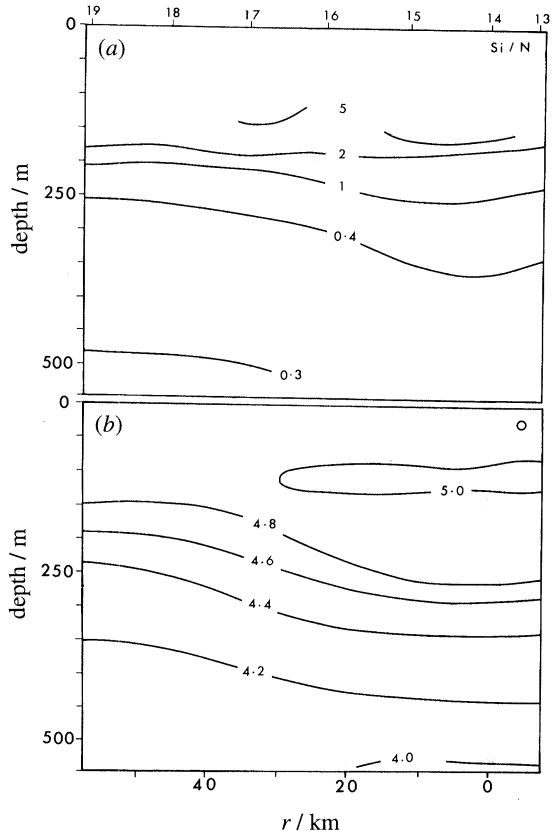

Figure 12. Vertical sections of (*a*) Redfield ratio (Si/N, silicate/nitrate), corresponding to figure 11 and (*b*) oxygen (ml l^{-1}). CTD stations marked.

increased, but chlorophyll 'a' maximum values were only *ca.* 0.1 mg m^{-3}. The general increase of oxygen concentration at the base of the seasonal thermocline is the result of biological activity (photosynthesis). Over the eddy centre, the thermocline is domed nearer the sea surface (figure 8) and the local increases in oxygen concentration here probably reflect a history of increased production in an earlier more favourable nutrient environment at increased light levels. In support of this, it is noted that, although low, the chlorophyll 'a' fluorescence values were elevated over the eddy core where the thermocline was shallower.

(*f*) *Horizontal sections*

Temperature contours in the horizontal plane show the horizontal structure of the eddy and may indicate the direction of water movement. The CTD and XBT profiles, together with SeaSoar runs, were used to derive both the horizontal distribution of temperature at selected depth levels and the depth contours of a selected isotherm. Maximum horizontal changes in temperature (salinity) occur at a depth near 250 m, and here the difference in temperature between the centre of the eddy and at a radial distance of *ca.* 50 km is *ca.* 2 °C. At a level of *ca.* 170 m, the horizontal gradients are absent and there is no temperature structure to indicate the streamlines of the flow in the region where the tangential currents have their maximum values (this contrasts strongly with the meddy situation (Pingree & Le Cann 1993*a*, *b*)). Above

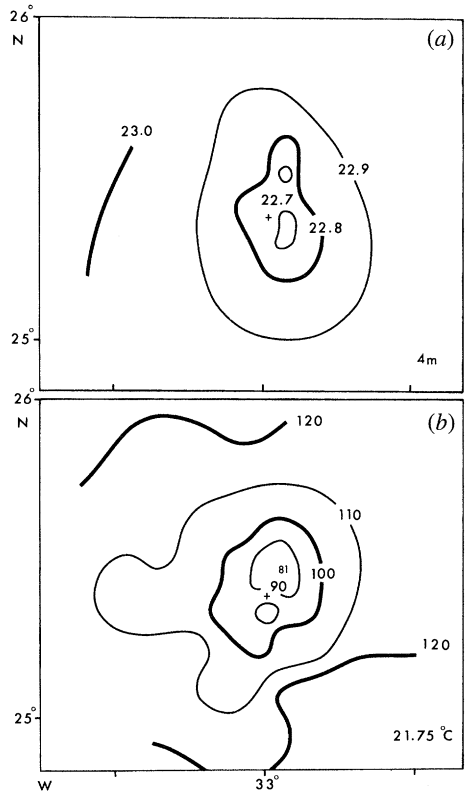

Figure 13. (*a*) Contours of sea surface (*ca.* 4 m depth) temperature (°C) showing sea surface cooling (22.7 °C, see also figure 8) over the eddy core (yeardays 352–356, 1993). (*b*) Depth (m) of the thermocline or 21.75 °C isotherm showing the upward doming of the thermocline associated with the eddy core (minimum value 81 m, marked). The cross at 33° W is the extrapolated eddy centre position (for yearday 352, time origin for station position corrections, see text for details) based on the track of buoy 3919. Measurements corrected for the westward movement of the eddy centre.

this level, water is cooler near the eddy centre. This doming of the isotherms (also isopycnals) may result in a cool patch extending to the sea surface in some situations, giving shallow anticyclonic eddies an infrared remote-sensing sea-surface signature.

In the Swesty situation, as already pointed out (see § 3 *c*), the mixed layer was well mixed (to about a thousandth of a °C) so the sea-surface cooling is not due to the doming of the isotherms. Underway measurements of sea surface (*ca.* 4 m) temperature show a cooler (*ca.* 0.3 °C) mixed layer near the eddy centre (figure 13*a*) and, in principle, it might be possible to track these eddies by remote sensing (infrared) for long periods across the ocean (in the absence of Lagrangian data (see, for example, Pingree & Le Cann 1992*b*)). It is expected that the cooling anomaly at the sea surface would be more marked in the summer period when lifting of the seasonal thermocline (with some stratification extending to near the sea surface) would enhance the surface cooling.

The centre of the seasonal thermocline, although just above the level of maximum upward displacement (see figure 8), is most accurately contoured, as small calibration temperature differences (in the XBTs) will result in minimum associated depth error. Figure 13*b* shows the depth of the 21.75 °C contour, which is centrally bound in

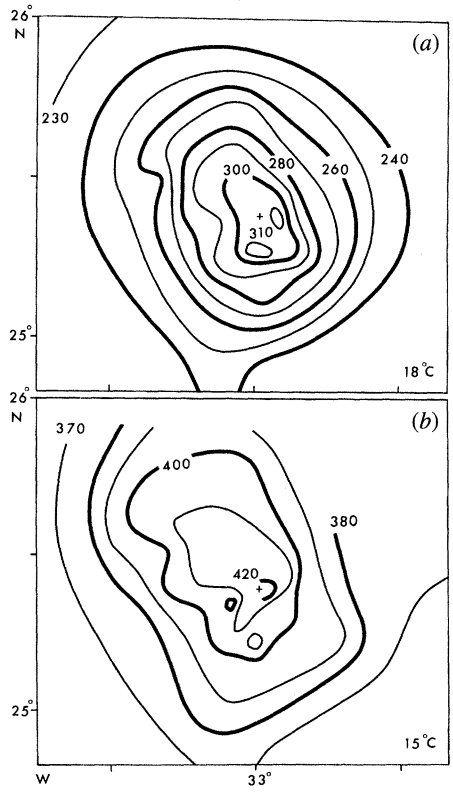

Figure 14. Contours showing the depth (m) of (*a*) 18.0 °C and (*b*) 15 °C isotherms.

the seasonal thermocline (see figure 8) and which shoals from a far-field (*ca.* 60 km radius) value of *ca.* 120 m to *ca.* 80 m over the eddy core.

The maximum downward displacement of isopycnals is well represented by the 18 °C contour with a far-field level of *ca.* 220 m, which descends to 310 m in the centre of the eddy core (figure 14*a*). The depression centre of the 18 °C isotherm appears to lie just south of the elevation centre at the thermocline level, indicating a slightly tilted structure (see figure 8). The contours appear elliptical with an elongation of shape along an axis *ca.* 150–330 °T.

The flatness of the structure means that displacements are rapidly attenuated with depth and the 15 °C isotherm at a depth of *ca.* 420 m, near the eddy centre, rises by *ca.* 50 m (*ca.* 55% of the displacement of the 18 ° isotherm *ca.* 100 m above) to a level of *ca.* 370 m (figure 14*b*) in the far field (*ca.* 60 km radius). Displacements were barely evident (*ca.* < 10 m) at 700 m depth, giving an overall vertical decay scale for temperature displacement of *ca.* 250 m below the core.

The 15 °C isotherm is tilted downwards to the northwest. This tilt is thought to reflect the westward movement of the eddy core. At the 400 m level, the oceanic isopycnals slope downward to the west (see figure 4) with a slope of about 1.0×10^{-4}. If to this we add a south–north slope (*ca.* 1.5×10^{-4}, see § 3 *c*) due to the westward flow, then the resultant slope will tilt downward to the northwest. The effect is less noticeable at the 18 °C level as the eddy flow is more marked, impressing stronger local radial gradients, and also the mean oceanic slope is probably weaker.

It is easy to show that tilts can produce elliptical depth contours for isotherms

(isopycnals). Consider the special case where the isotherm surface is the surface of a right-circular cone and all the depth contours for the fixed isotherm are circular. This could occur with a circular tangential orbital velocity that was independent of radius or, more realistically, in the region of maximum azimuthal current where the eddy tangential current structure is flat. If the coned region is now tilted (as a result of westward geostrophic flow of the core) then a level plain cuts the cone (isotherm surface) at an angle giving a conic section for a level contour. For a central region that has near constant relative vorticity, the cone becomes a paraboloid of revolution and an imposed tilt produces circular contours again, but their centres are displaced in the direction of downward tilt.

4. Results: current structure

(*a*) *Geostrophic/ADCP currents, vertical structure and azimuthal transport*

For stationary radially symmetric conditions, the gradient equation can be used to derive the horizontal azimuthal current structure. Changes in the gradient current, $v(r, z)$, in the vertical (z) are related to horizontal changes of density with radius, thus

$$\rho \frac{\partial v}{\partial z}(f + 2v/r) = -g \frac{\partial \rho}{\partial r}, \tag{4.1}$$

where ρ is the density and r is the horizontal radial distance from the eddy centre. With a deep reference level (2000 m say), the gradient currents near the eddy core will increase up to a depth of near 175 m (i.e. near level isopycnal) and then start to decrease (see figure 9*a*).

Geostrophic currents (i.e. with $v/fr \sim 0$ in (4.1)) and azimuthal transports were derived from dynamic heights calculated for each CTD station using a reference level of 2000 m. The results (figure 15) show maximum currents at a depth of about 175 m, which extend to the sea surface but diminish rapidly with depth, showing little coherent eddy structure below a depth of *ca.* 800 m. The azimuthal geostrophic transport was 3.0 Sv to a radius of 50 km and *ca.* 3.7 Sv to a radius of *ca.* 100 km (average of CTDs 20 and 7, figure 2, with the eddy centre). These transport values are much smaller than most reported eddy transports for mesoscale eddies; for example, meddies *ca.* 10 Sv to a radius of 50 km (see table 2), and it is perhaps remarkable that such a small transport feature has travelled so far and survived for so long. Reasons for the particularly low transport stem from the flatness of the eddy with small vertical decay scale (currents fall to e^{-1} values at a *ca.* 300 m increase in depth), the relatively slow (but f dependent) tangential currents (maximum values *ca.* 16 cm s^{-1}) and the shallowness (dynamic centre near *ca.* 175 m, i.e. less transport above than below) of the core of this subtropical eddy.

On much shorter time scales, the ship's hull mounted ADCP can be used to derive estimates of the eddy current structure, but the results will include contributions from higher frequency components such as inertial waves. ADCP current profiles from the ship's hull-mounted transducers were derived over about 4 h averages when the ship was near stationary at the CTD stations and the results were similar to the geostrophic section for the useful depth range (*ca.* 300 m) of the 153 kHz transducers. The ADCP results confirmed that the maximum currents occurred at a depth of *ca.* 175 m and that the eddy centre was within a few km (4.5 km west) of CTD 14 at 200 m (figure 16). The maximum currents were 16 cm s^{-1} at a radius of *ca.* 30 km and an inner core of radius *ca.* 5 km appeared to be in near solid-body rotation with a

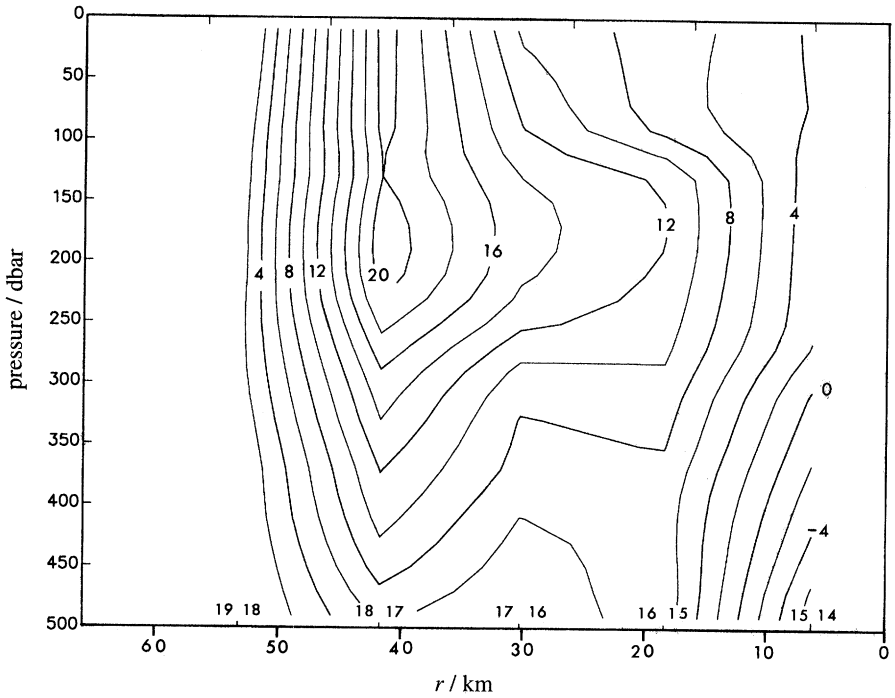

Figure 15. Vertical section showing the uncorrected geostrophic velocity component (cm s^{-1}) normal to the line of CTD stations against pressure (dbar). Positive values are directed into the plane of the paper (or north). The centre positions of the CTD station pairs used to derive the geostrophic currents are indicated on a true distance scale, r (km), from the position of CTD 14. To correct for westward eddy movement, values of r at the intervals indicated should be decreased by 4% to 96% and the contour values increased by 4%; i.e. the transport between positions is conserved. Geostrophic values have maximum values at a pressure of *ca.* 175 dbar.

period of *ca.* 5 d. The azimuthal transport for the ADCP section (to a depth of 300 m and radius of 60 km) was 1.4 Sv, consistent with the low values derived from the geostrophic estimates. The mean westerly velocity component to a radius of 50 km and in the depth range 50–250 m, reflecting eddy translation, was determined as 2.7 cm s^{-1}, consistent with the value (3.7 cm s^{-1}) derived over a much longer period of time (*ca.* 16 months) and in closer agreement with a value of 3.1 cm s^{-1} determined from the buoy trajectories over a 15 d period just after the hydrographic survey.

(*b*) *Buoy trajectories*

Eddy kinematics from the drogued buoys have been derived over much longer integration timescales based on simple relationships, but higher frequency velocity components have also been derived (see § 9). The tangential (azimuthal) velocity v, at a radius r, was derived from the buoy period T, and the displacement of the buoy's track D, in a direction normal to the generally westward movement of the eddy (i.e. $D \sim 2r$), with

$$v = \pi D/T. \tag{4.2}$$

The vertical component of vorticity ζ and rate of strain η are defined as

$$\zeta = \frac{1}{r}\frac{\mathrm{d}(rv)}{\mathrm{d}r}, \tag{4.3}$$

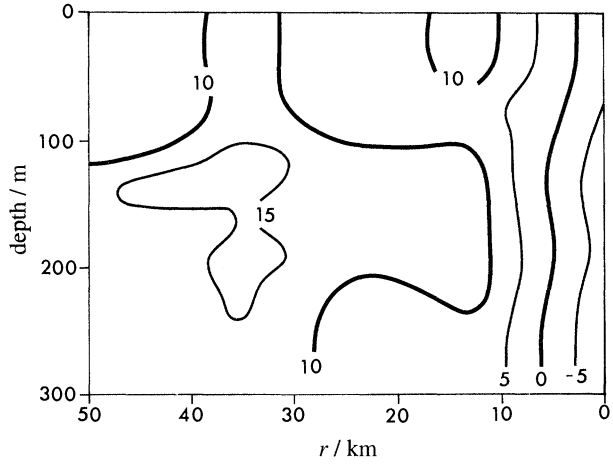

Figure 16. Contours of north component of ADCP current (cm s^{-1}). The vertical section is depth (m) against distance r in km from CTD 14. Currents change sign at $r \sim 4.5$ km near the eddy centre.

$$\eta = \frac{\mathrm{d}v}{\mathrm{d}r} - \frac{v}{r}. \tag{4.4}$$

The normalized (by f) relative vorticity, ζ/f, for an eddy in near solid body rotation is

$$\frac{\zeta}{f} = \frac{1}{fr}\frac{\mathrm{d}(rv)}{\mathrm{d}r} \sim -\frac{4\pi}{Tf}, \tag{4.5}$$

where T is now the solid-body rotation period and f is the coriolis parameter. Equation (4.5) is useful when a buoy is near the eddy centre and the eddy centre or central core is in near-solid-body rotation, as the vorticity can then be estimated from the central rotation period of the buoy alone.

The tracks of the four Argos buoys show the eddy movement from *ca.* 25° W to about *ca.* 41° W (figure 1) and represent a total of about *ca.* 760 buoy-days (or *ca.* 2 buoy-years) under the influence of eddy motion with about seven position fixes a day, giving some *ca.* 5300 position values for velocity values. For most purposes, position data or velocity data can be used equally. A velocity presentation is simply a convenient way of preferentially attenuating the low-frequency components of the signal (in the present context we want to examine the eddy motion and the ocean waves or low-frequency motions are merely a nuisance). The velocity results (figure 17) do not show perfect circular motion; rather they give the impression of a rather wobbly structure which we know remains coherent as a whole and which is untangled in the subsequent sections. The maximum daily speed over about a two-year period was only *ca.* 30 cm s^{-1}.

Summaries of the individual drogued-buoy results are given in table 3 and the drogued-buoy movements are referred to by buoy number. Positions from drogued buoy 3346 are split into two portions, 3346a and 3346b. The first short piece (3346a) appears to be a first encounter with the eddy near 23° N in February 1993. This slightly earlier position for the eddy is consistent with an extrapolation of the track of the eddy centre (*ca.* 100 km $month^{-1}$) and the temperature of the eddy core (see § 6). 3346b was in the eddy continuously from the end of April 1993 to the end of the year (for *ca.* 241 d), and executed orbits at a radius of about 18 km in about *ca.* 10 d for the first half of this period. It then moved to a larger radius of about 65 km,

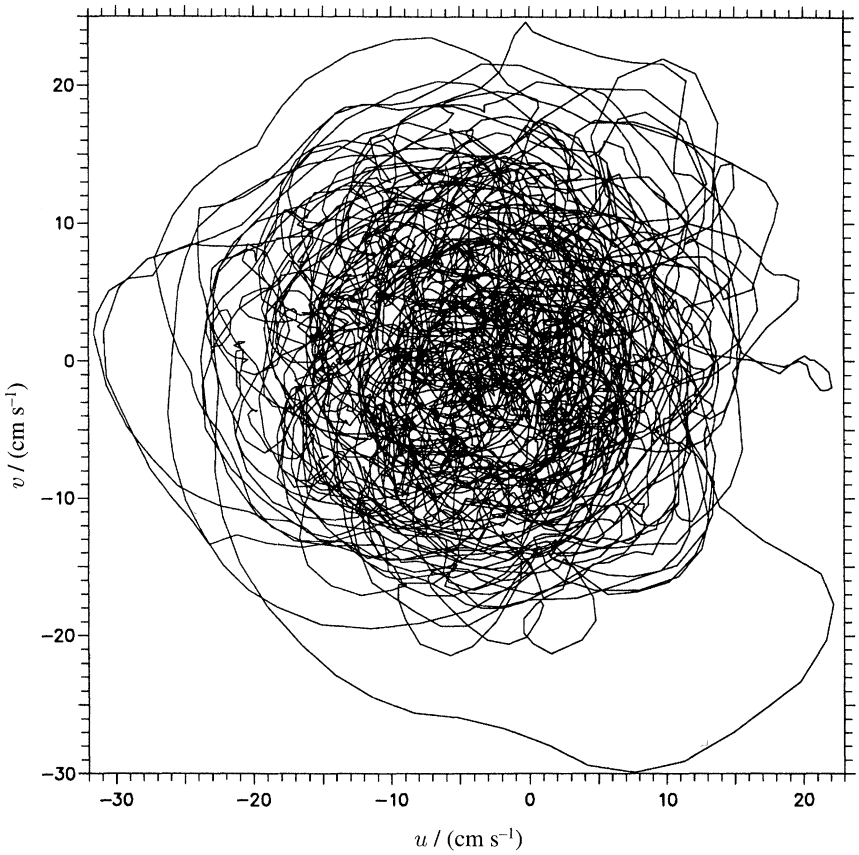

Figure 17. Velocity values (12 h averaging of position data) of all buoys in the eddy (*ca.* 2 buoy-years). Note centre is displaced as eddy is translating westward.

where the rotation period was about 45 d. The innermost orbits experienced by 3346 had a period of $T = 8$ d and this rotation rate was used to estimate an initial core vorticity, $\zeta/f = -0.29$ from (4.5) (table 3). The outermost orbits showed that the eddy was slowing.

Before the recovery of buoy 3346 from the eddy (on 22 December), buoys 1811, 3915 and 3919 were deployed (with drogues set at 200 m) and these three buoys were in the eddy together for about *ca.* 125 d, orbiting at typical radii of 25 km and period of *ca.* 12 d, and with a central rotation period still about 8 d (figure 1). 1811 and 3919 lost the eddy almost simultaneously from the northern flank, while, at a radius of about 65 km, 1811 made a small (*ca.* 10 km) cyclonic loop before exiting. It is possible that a portion of the eddy became detached near the edge of the eddy. The earlier observations (3346b) showed that a drogued buoy could be carried along with the eddy to a radius of about 65 km and it is probable that the eddy had now diminished in size. Buoys 1811 and 3919 then moved south (at an initial speed of *ca.* 5 cm s^{-1}), showing progressively less influence of the westward moving eddy. It seems probable that during the encounter with the southerly stream at 35.5° W, those buoys (1811, 3919) near the eddy's extremity were dragged out of the water mass actually moving with the eddy. It is remarked that the eddy itself appeared to be advected south (*ca.* 45 km) by the stream, but subsequently recovered its latitude, in about 50 d (see

Table 3. *Summary of drogued buoy trajectories in the influence of Swesty as it travelled westward near the latitude of* 25° N *with a mean speed of* 3.7 cm s^{-1}

Argos buoy number	3346a	3346b	1811	3919	3915
drogue depth (m)	200	200	200	200	200
entry near Longitude ° W	22.8	24.8	33.1	33.0	33.3
date	17.2.93	25.4.93	19.12.93	21.12.93	19.12.93
yearday 1993	48	115	353	355	353
leaving near longitude ° W	22.8	33.6	35.8	35.5	41.3[a]
date	4.3.93	22.12.93	25.4.94	24.4.94	12.9.94
yearday 1993	63	356	480	479	620
duration in eddy (d)	15	241[c]	127	124	267[b]
approximate number of loops	$\approx \frac{1}{4}$	14	10	9	36
maximum daily speed cm s^{-1}	—	22	30	20	29
kinetic energy[d] (cm^2 s^{-2})	—	69	80	53	81
total variance (cm^2 s^{-2})					
east–west	—	80	93	48	87
north–south	—	58	67	57	74
mean west component (cm s^{-1})	—	4.2	2.4	2.3	3.5
rotation period[e] (d)	—	8	9	8	5
(yearday) 1993		(152)	(380)	(370)	(570)
core vorticity $-\zeta/f$		0.29	0.27	0.28	0.47

[a]Drogue loss position.
[b]267 d drogued (see text for details).
[c]This buoy (3346), which was initially deployed at 30°00′ N, 28°28′ W on 7 March 1992 over the Great Meteor Tablemount, was recovered on 22 December 1993 (after the deployment of buoys 1811, 3915 and 3919) with drogue intact (but with marine growth) after 655 d at sea (and the drogue was used again later (2 d) on a further long-term drogued buoy deployment.
[d]Kinetic energy derived from velocity components based on position intervals at 12 h and includes the mean motion.
[e]Based on two or three innermost orbits, centred near the given yearday.

figure 1, near months 4–7, 1994). Clearly, it is important to have measurements of water movement in the region exterior to the eddy and the subsequent movements of 1811 and 3915 have been used to provide some background properties (table 4).

3915 was within 20 km of the eddy centre when the other two buoys were left behind and so would have been harder to remove by a surface current (Pingree & Le Cann 1991). The buoy's track shows that, rather than slowing, the eddy core appeared to speed up. A 6 d central rotation was observed near yearday 478. This buoy appeared to work its way to the eddy centre near yearday 550 and a 5 d rotation was observed near yearday 570 (table 3). A minimum central rotation period of 5 d gives a maximum negative central core vorticity $\zeta/f = -0.47$. With the buoy presumably near the eddy centre, looping motions were less evident during this latter period and further evidence would be desirable confirming that the drogued buoy was still with the eddy. Oscillations were more evident in the buoy's velocity components,

Table 4. *Flow characteristics external to Swesty*

Argos buoy number	1811	3919
drogue depth (m)	200	200
yeardays	480–646	479–662
duration (d)	166	183
maximum daily speed (cm s^{-1})	14	14
kinetic energy (includes mean) (cm^2 s^{-2})	28	29
mean west component (cm s^{-1})	−0.3	3.2
mean north component (cm s^{-1})	−3.9	−3.1

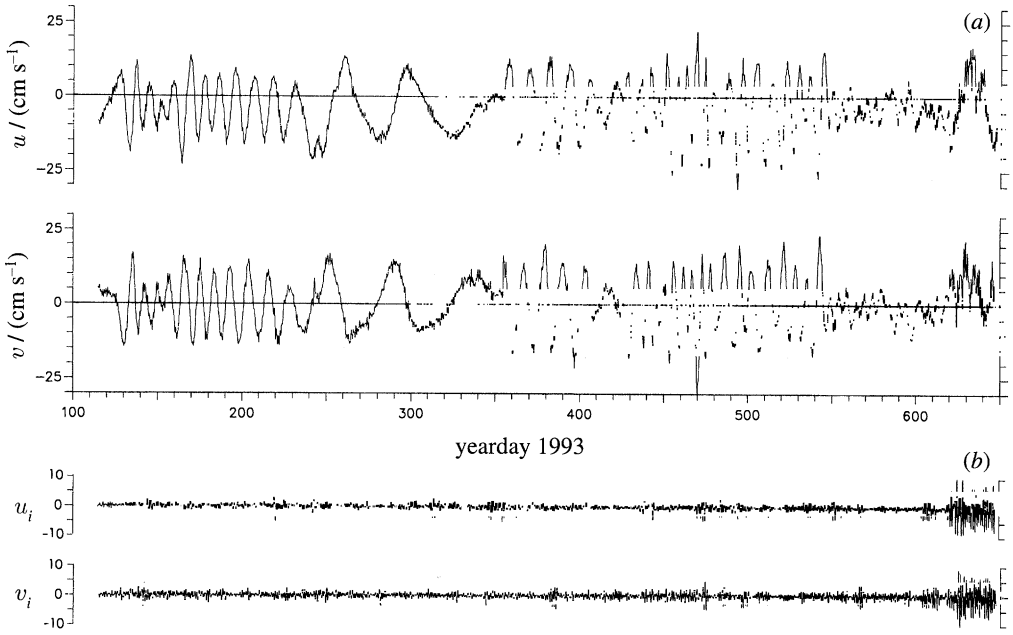

Figure 18. (*a*) East (u) and north (v) components of buoy (3346 and 3915) velocity (cm s^{-1}) derived from 12 h differences in position against yearday. (*b*) Corresponding inertial components of the motion, u_i and v_i (cm s^{-1}), derived from U, V in (*a*).

which showed a *ca.* 5 d periodicity. Buoy 3915 lost its drogue on yearday 620 (see § 9).

A buoy velocity record covering a *ca.* 530 d period is shown in figure 18, but it is clear that further *ca.* 125 d records from 1811 and 3919 exist for the central period (yearday *ca.* 355–480). Periodicity (i.e. evidence for eddy motion), although variable in period and at times with higher frequency variance, can be seen in the velocity components to about yearday *ca.* 620.

The mean westward flow due to both the ocean and the eddy is clearly seen in the displacement of the mean level of the east component (u, figure 18) of the Lagrangian flow. There is little suggestion of the Lagrangian effect that might be expected when

following a westward-moving particle in the field of flow of a circular eddy pattern that is moving with westward phase speed rather than truly advecting (Flierl 1981; Pingree & Le Cann 1991). Although water in the flow pattern of the central core will be advecting, water in the exterior eddy regions will not be able to keep up with the eddy flow pattern. The Lagrangian u component in the exterior eddy region might be expected to be more peaked at maximum eastward flow with respect to conditions during maximum westward flow. Saw-tooth asymmetry would be expected for the Lagrangian north component, v. Some asymmetry occurs between yeardays *ca.* 250–350.

The centre rotation period of the eddy suggests that the interior region of the eddy has speeded up. Table 3 does not shows a clear trend of increasing kinetic energy, as buoy 3915 appeared to work its way into the eddy centre where the azimuthal currents decrease. Developing on this line of argument, suggesting that the centre of the eddy was speeding up, the velocity components of the buoys have been grouped into three portions: an initial period (from yearday 115 to 240; 3346), a central period (from yearday 365 to 445; 1811, 3915 and 3919) and a later period (from yearday 445 to 565; 3915). The latter period does not include the end of the trajectory of buoy 3915, where the looping motions were not so clearly apparent. In addition to velocity components, displacement components were derived by subtracting from each buoy's position the estimated position of the moving eddy centre. The position of the eddy centre was approximated by averaging each buoy's position over a sufficiently long period, and, after a few trials, a 24 d running mean was adopted. For the central period when the three buoys were in the eddy together, a better estimate for the eddy centre can be found by averaging the 24 d running mean positions of all three buoys. This was also done and the overall conclusion resulting from this approach was much the same. However, for consistency when comparing the central results with those earlier and later, the buoy track displacements and velocity components were all derived in the same manner. The results (figure 19) show an increasing RMS velocity deviation, $v' = 11$, 12 and 14 cm s^{-1} over the three period, which is not fully compensated for by RMS position displacement, $d' = 19$, 21 and 18 km, giving characteristic periods, $2\pi d'/v' = 13$, 13 and 9 d. Overall, the results show that the tangential speed in the central region (*ca.* 20 km radius and at the 200 m depth level) has increased by about 25% over a mean period of about 300 d.

(*c*) *Tangential current structure at the core depth* (*ca.* 200 m)

The radial distribution of azimuthal current derived from the buoy trajectories just after the hydrographic survey (figure 20*a*) can be compared with geostrophic- (figure 15) and ADCP-derived values (figure 16). The gradient current values will be rather larger near the eddy centre, where maximum increases of $(1+\zeta/2f)^{-1} \sim 1.15$ occur. Differences between geostrophic estimates and buoy-derived values at larger radii might be attributed to variable horizontal density structure (all of which will not be geostrophically balanced anyway, e.g. internal waves), which is effectively averaged out using (4.2) for the buoy derived values. The eddy is in near-solid-body rotation to a radius of 10 km at most and the maximum tangential currents are correspondingly low; *ca.* 16 cm s^{-1} at a radius of 30 km.

This value (*ca.* 16 cm s^{-1}) is particularly low compared to say Gulf Stream rings, Agulhas eddies or North Brazil retroflection eddies, which can reach values of 80 cm s^{-1} at a radius of 125 km (Richardson *et al.* 1994). Northeast Atlantic anticyclonic eddies (e.g. east Thulean Rise eddies (Pingree & Le Cann 1991)) show

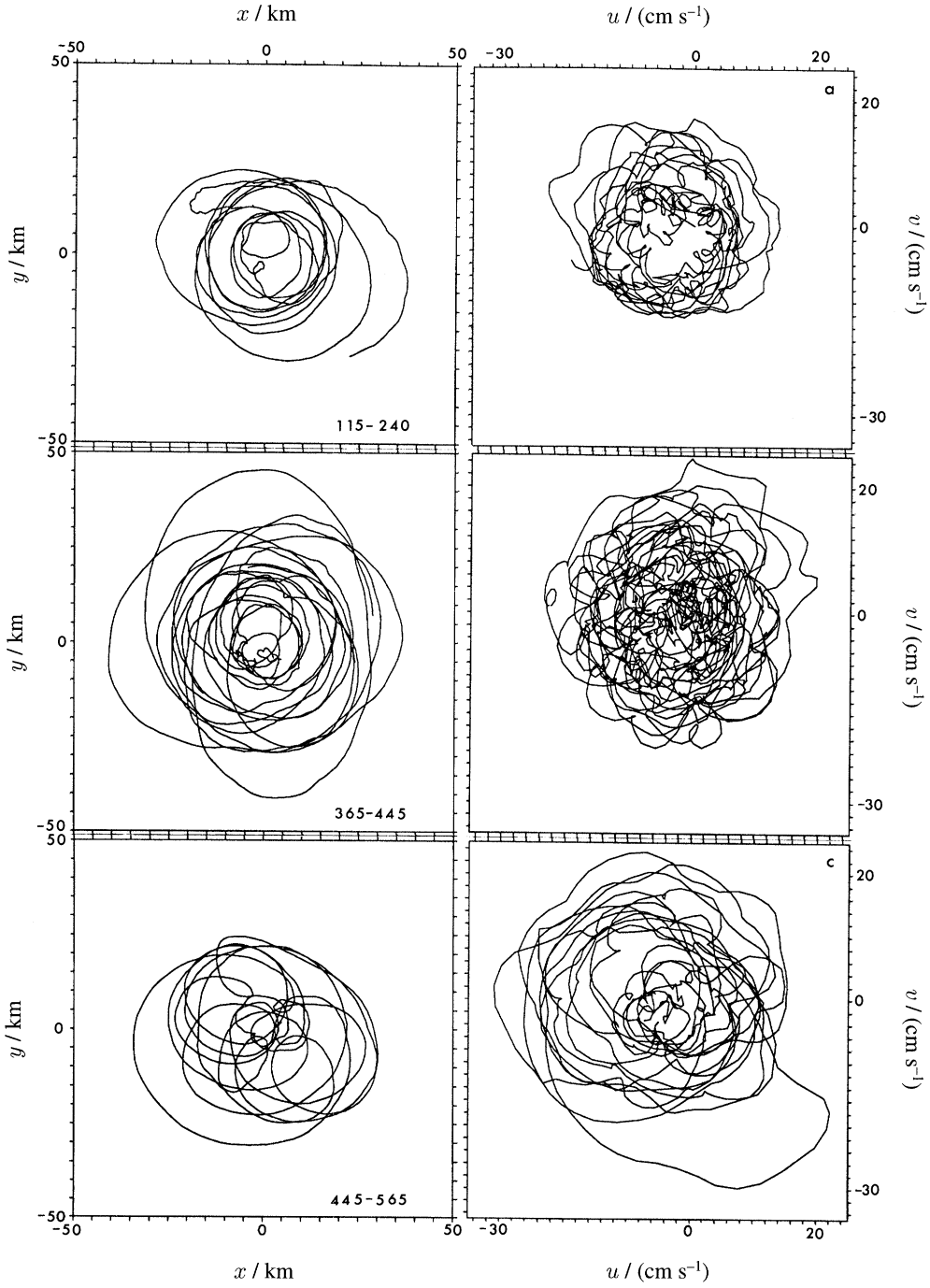

Figure 19. Buoy displacements (x east, y north in km) and velocity components (u east, v north in cm s^{-1}) for (a) initial 115–240, (b) central 365–445 and (c) later period 445–565 yearday (see text for details).

near surface currents of 45 cm s^{-1} at a radius of 55 km and the maximum tangential

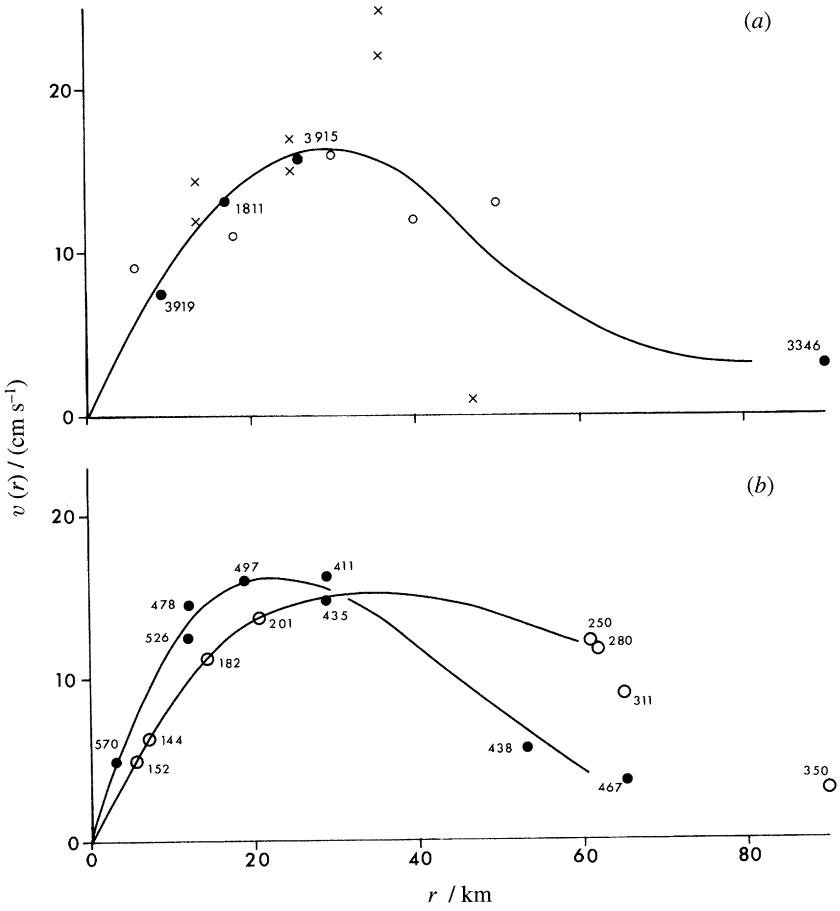

Figure 20. (*a*) Curve of mean tangential speed, $v(r)$ (cm s^{-1}), against eddy radius, r (km), at a depth of 200 m for the survey period (yearday $\sim$ 355). Open circles, ADCP estimates; crosses, geostrophic and gradient (upper cross) values. Values shown by dots were derived from drogued buoys 3346, 1811, 3915 and 3919 (buoy numbers annotated). The idealized curve places more reliance on the buoy values. The two external geostrophic values can be averaged (i.e. estimate now based between CTDs 17 and 19, see figure 15). (*b*) Curves of mean tangential speed, $v(r)$ (cm s^{-1}), against eddy radius, r (km), at a depth of 200 m for an early period (open circles, buoy 3346) centred near yearday $\sim$ 190 and a later period (dots, buoys 3915, 1811, 3919) centred near yearday *ca.* 480 about 300 d later. Yearday 1993 marked.

currents in the few surveyed eddies of known origin are given in table 2, where Swesty is seen to be conspicuously the weakest, though comparable in radial size.

An initial radial distribution of azimuthal current structure at 200 m depth, $v(r, 200)$, was derived from 3346b using (4.2). An 8 d rotation period centred near yearday 152 (table 3) gave an estimate of 5.0 cm s^{-1} for a radius of 5.5 km. 10 d rotation periods were characteristic of larger radius orbits (*ca.* 18 km). A value of *ca.* 12 cm s^{-1} occurred at a radius of *ca.* 60 km near a central yearday of 250; the curve comprising these values is shown in figure 20*b* and broadly represents conditions centred near yearday *ca.* 200.

Values at large radii become weaker with time, e.g. 9 cm s^{-1} at a radius of 65 km for yearday 311. The value of 3.2 cm s^{-1} at *ca.* 90 km for near yearday 350 for buoy

3346 was an estimate based on the position, where the eastward movement of this buoy due to the rotation of the eddy appeared to just balance advection to the west, with the buoy moving slowly north near the end of its trajectory (figure 1). This value will be an overestimate if the eddy pattern is propagating rather than advecting at a large radius. Subsequent changes to the outer structure are for the period where 1811 reached a large radius (yearday 438) and when 3919 and 1811 started to leave the eddy (yearday 467).

While the outer region of the eddy was slowing or getting smaller, the inner region appeared to be speeding up and rotating faster. A near central rotation of 5 d was determined near yearday 570 for 3915. The second curve shown in figure 20*b* broadly represents conditions for near yearday *ca.* 500 and the difference in the two curves is the extent of the changes over a *ca.* 300 d period. The bias in the timings means that the changes are over a *ca.* 400 d period for the eddy centre and *ca.* 200 d for the exterior region.

The results at 200 m depth suggest a structure that was rotating faster internally but slowing and diminishing in size outwardly. However, the faster central rotation could be interpreted as providing evidence for subduction and caused as the depth of maximum currents deepens towards the drogue depth (*ca.* 200 m) over the observation period. This effect might be broadly estimated as resulting in a *ca.* 10% increase in azimuthal current (see figure 15) and expected to be relatively more marked during the early stages of eddy evolution. Similarly, the exterior regions of the eddy may have had a more rapid decay than suggested from the observations over the *ca.* 300 d period.

(*d*) *Summary structure of radial distribution of tangential current*

A simple approximate analytical velocity function $v(r, z, t)$, summarizing the idealized eddy structure, is a Rayleigh distribution with further Gaussian decay in the vertical:

$$v(r, z, t) = (Vor/\,Ro)\exp -(r/\,Ro)^2 \exp -[(z - Zo)/\,Lo]^2, \tag{4.6}$$

where r is the radial distance, z is depth and Ro, Vo, Zo and Lo are time-dependent scales. For the central period, with $Ro = 42.4$ km and $Vo = 37.3\ \mathrm{cm\ s^{-1}}$ say, a velocity maximum of $16\ \mathrm{cm\ s^{-1}}$ occurs at $r = Ro/\sqrt{2} = 30$ km, and a normalized relative vorticity at the centre of the eddy core, $\zeta/f = -0.3$. Zo is 180 m and, with a vertical width scale, Lo, of *ca.* 300 m, the currents will fall to e^{-1} at a depth of *ca.* 500 m and are effectively absent (*ca.* 2%) at a depth of 800 m. Equation (4.6) integrates to 3.4 Sv (*ca.* 2.6 Sv to 50 km) and could be made to match the geostrophic transport by adjustment to Lo but the agreement is already within the variability of transport estimates (§ 4 *a*). Vo appears to have changed little, and changes in Ro, $\mathrm{d}\,Ro/\mathrm{d}t \sim 0.1\ \mathrm{cm\ s^{-1}}$, are responsible for the observed changes. Zo and Lo would be expected to be smaller initially (i.e. an eddy formed at the surface followed by subduction, see § 6). The analytical form is convenient to characterize the eddy velocity structure for the central period and useful for future analytical and numerical modelling studies aimed at investigating the dynamic properties of a Swesty.

(*e*) *Potential vorticity*

The stability structure N and the vorticity derived from the current structure have been used to derive a vertical section of potential vorticity Q, where

$$Q = N^2 f(1 + \zeta/f)/g. \tag{4.7}$$

The distribution of Q for the central period (figure 21) is similar to N (figure 9*b*). The main effect of the vorticity term in (4.7) is to stretch (vertically) the structure

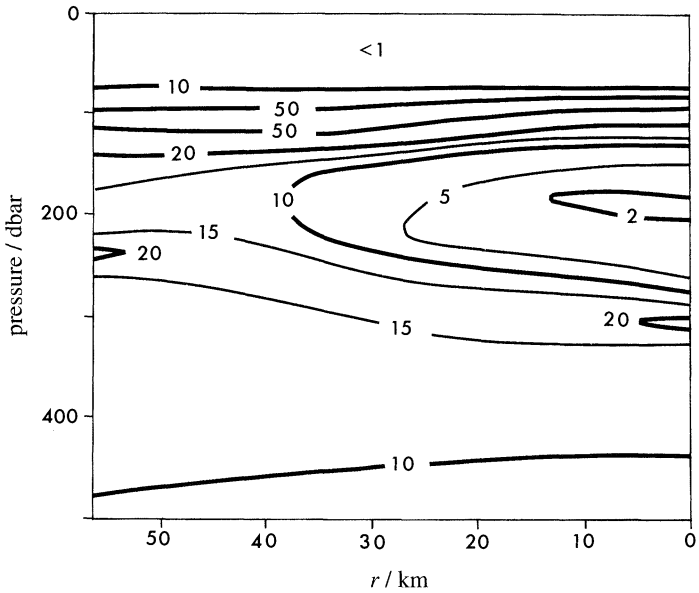

Figure 21. Vertical section, with pressure (dbar) against radial distance (km) measured from CTD 14, showing contours of potential vorticity for the central period in units of 10^{-11} rad ms^{-1}. Swesty is seen squashed below the eroding seasonal thermocline (maximum values *ca.* 60). Minimum values (*ca.* 1.5) occur in the core at a pressure of 195 dbar.

near the centre of the eddy core which has a minimum value of 1.5×10^{-11} rad ms^{-1} (comparable with meddies, *ca.* 3×10^{-11} rad ms^{-1} for Meddy Sharon (Schultz Tokos & Rossby 1991); *ca.* 1.2×10^{-11} rad ms^{-1} determined for Meddy Bobby (Pingree & Le Cann 1993*a*); *ca.* 2.1×10^{-11} rad ms^{-1} for Smeddy Tagus (Pingree & Le Cann 1993*b*)), see table 2.

In this potential vorticity view, the eddy is clearly seen as a low, centred at *ca.* 200 m, against a background of high potential vorticity (i.e. the upper permanent thermocline). The contours in the central region of the eddy act to inhibit isentropic exchanges and insulate the core water properties from the surrounding water. The potential vorticity at the *ca.* 200 m level changes by an order of magnitude (*ca.* 1.5×10^{-11} rad ms^{-1} in the eddy core to *ca.* 18.0×10^{-11} rad ms^{-1} at a radius of *ca.* 100 km). At *ca.* 180 m depth (level isopycnal), the potential vorticity changes by a factor *ca.* 6 to a radius of 50 km. These relatively large changes in potential vorticity guarantee the survival of the eddy, despite its relatively small transport.

The low aspect ratio of the Q structure (0.2%) reflects the fact that the eddy is formed or moving at a relatively low latitude and squashed in the near surface water where $N \sim 3$ cph is larger and also the near presence of the seasonal thermocline. Initially, a surface formation will tend to result in the production of a half-structure. Swoddy F90a (table 2), also a surface eddy, had a relatively low aspect ratio *ca.* 0.45% ($N \sim 1.5$ cph external to the eddy core at *ca.* 150 m and this eddy moved at a latitude near 45° N).

5. Eddy translation

Anticyclonic eddies are expected to move westward due to the variations of coriolis parameter with latitude or beta effect (Nof 1981) and southward due to both nonlin-

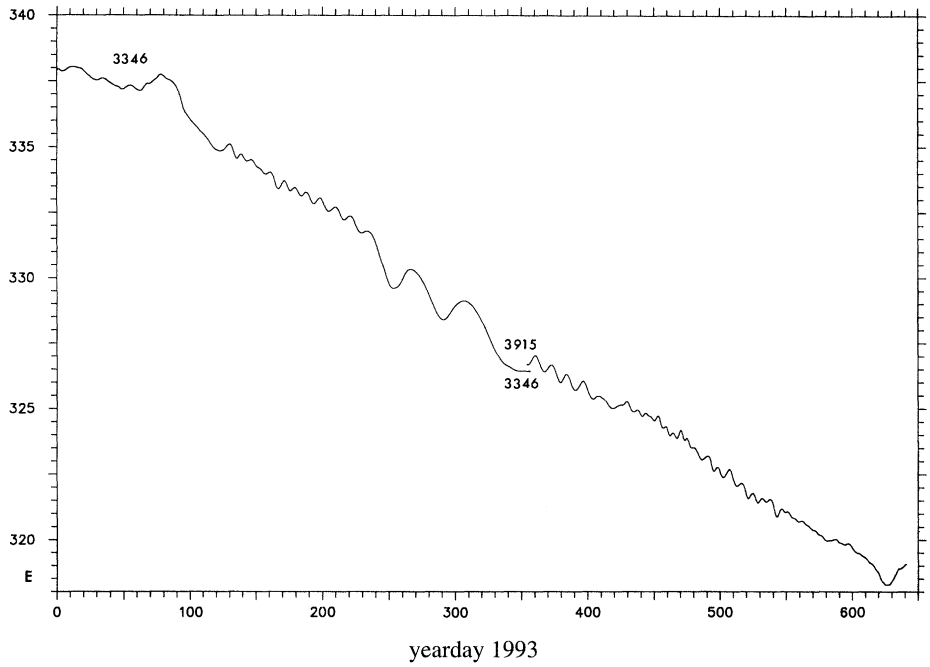

Figure 22. Longitude (degrees east) displacement of buoys 3346 and 3915 against yearday 1993. Buoy 3346 was perhaps first in the eddy near yearday 50 and then continuously from yearday 115–356. Buoy 3915 was positioned nearer the eddy centre and in the eddy on yearday 353 but lost its drogue on yearday 620.

earity (Cushman-Roisin *et al.* 1990) and mixing and decay (Colin de Verdiere 1992). The actual observed movement of an eddy will also depend on advection or ocean currents and the influence of other eddies. Despite the changes in velocity structure $v(r, z, t)$, the translation velocity of the eddy, U, changed little over the observation period (figure 22, note we are now examining position rather than velocity as the low-frequency position components of the motion are enhanced); a rotary clockwise *ca.* 200 d periodicity may be evident (see figure 1 for north–south tendencies).

In this section, aimed at determining both how much of the eddy's westward movement is due to the ocean and how much is due to self-propagation and whether or not the eddy is maintaining a latitude against the southward component of the Subtropical Gyre, it is important to realize that direct current measurements for the ocean at 200 m near 25° N do not exist or have not been published. Indeed, an important gap in the direct measurements (at *ca.* 200 m) has been identified and the indirect or theoretical estimates of the strength and direction of the mean flow of the Subtropical Gyre given below still need support from long-term observation.

(*a*) *Westward component*

The mean westward eddy speed was 3.7 cm s^{-1}, which is relatively fast (table 2). Note the mean westward speed from the mean of the buoys (table 3) is slightly less (*ca.* 3.1 cm s^{-1}), implying that as a buoy leaves the eddy it is left behind and that the eddy is moving westward relative to the flow of the Subtropical Gyre. The Subtropical Gyre has a westward component at a latitude of 25° N and the westerly movement at 200 m depth, gauged from the mean westward movement of buoys 1811 and 3919 after they left the eddy, was *ca.* 1.5 cm s^{-1} (*ca.* 350 d mean, both buoys,

table 4), so this rough estimate suggests *ca.* 60% of the eddy's translation is due to self-propagation. The south component of the mean eddy translation was 0.2 cm s^{-1}, giving an aspect ratio (on the curved surface of the Earth) of *ca.* 0.06.

Other indirect estimates of the mean surface westerly flow for the Subtropical Gyre in this region are available. Olbers *et al.* (1985) show southwest directed (i.e. an aspect ratio of near one) currents with speed near *ca.* 2 cm s^{-1}, giving *ca.* 1.4 cm s^{-1} for the westward component at a depth of 100 m in this region. The eddy actually passed through the beta triangle region of Armi & Stommel (1983), centred at 27° N, 32.5° W, making a *ca.* 800 km cut. At the triangle centre and at 194 dbar, these authors give a westward component of 0.6 cm s^{-1} and a southward component of 0.8 cm s^{-1}, with resultant *ca.* 1.0 cm s^{-1} (Olbers *et al.* (1985) suggest a resultant of 1.4 cm s^{-1} directed southwesterly at this position based on climatological spirals). The eddy centre passed about 150 km to the south of the centre of the triangle (i.e. nearer to the North Equatorial Current (NEC)), where the dynamic height gradients (in north–south direction) are larger and so the above westward values might be increased by a factor of nearly two. Overall, we deduce a westward ocean flow of *ca.* 1.5 cm s^{-1} for an eddy moving near 25° N based on historical geostrophic calculations. The value for the eddy propagation speed is then *ca.* 2.2 cm s^{-1}, larger than the value of westward movement (*ca.* 1.5 cm s^{-1}) estimated in § 3 *c* and also larger than a theoretical estimate for the beta-induced motion given below.

Estimates for the beta-induced motion give a westward eddy speed, *c*, of order $c \sim \beta R_d^2 \sim 0.7$ cm s^{-1}, with $\beta = 2.1 \times 10^{-11}$ ms^{-1}, $R_d = \{g' H_1 / f^2\}^{1/2} = 18$ km, an internal reduced gravity $g' \sim 0.005$ ms^{-2} and an exterior interface level of $H_1 = 250$ m using the derivations and assumptions adopted by Cushman-Roisin *et al.* (1990). This value (0.7 cm s^{-1}) is too small to account for the overall westward movement and either a further theoretical contribution needs to be found or the westward flow of the Subtropical Gyre increased to *ca.* 3.0 cm s^{-1} at the latitude of *ca.* 25° N. The latter could occur if the Subtropical Gyre (or NEC) was displaced northward in 1993/1994.

(*b*) *Southward component*

Although decaying or getting smaller, this eddy has not moved significantly south (compared to say, meddies: the southward speed of Meddy Sharon was 1.8 cm s^{-1} (table 2), see Armi *et al.* 1989; Richardson *et al.* 1989) and other effects appear to be balancing the southward component of the eddy translation. Perhaps changes of structure, increasing the central rotation speed, and sinking are acting to oppose any marked southward component.

Is the eddy integrating the southward flow of the Subtropical Gyre (a Sverdrup integrator) as it moves relatively quickly westward or is it swimming northward, compensating for latitude changes (an *f* compensator)? The meridional component M_y of the vertically integrated Sverdrup transport is given from the mean field of wind stress curl $\nabla \wedge \tau$ (vertical component) using

$$\beta M_y = \nabla \wedge \tau. \tag{5.1}$$

Summing the transport westward (Gill 1982; Isemer & Hasse 1987) over the eddy track from 23° W to 42° W gives *ca.* 12 Sv (rather less than that found from the section at 25.5° N, *ca.* 12 Sv from 23° W to 34.5° W, figure 4). Assuming this wind influence on the Subtropical Gyre is distributed evenly through the upper 500 m, then a mean representative southward velocity is *ca.* 1 cm s^{-1} (comparable with the values

already given from historical hydrographic data) with a value of *ca.* 2 cm s^{-1} nearer the sea surface using the present hydrographic data (see § 3 *a*). A value of 1.0 cm s^{-1} is considerably larger (×5) than the southward speed of the eddy, suggesting that the eddy is resisting changes in latitude. After leaving the eddy, buoys 1811 and 3919 moved south at a mean speed of *ca.* 3.5 cm s^{-1} (350 d average, table 4), so the actual local southward velocities experienced by the eddy may have been even larger. Once again we note that we do not have a direct measurement of the mean southward component of flow of the Subtropical Gyre at a depth of *ca.* 200 m at this latitude (*ca.* 25° N). While it appears that the eddy can resist local variability in the flow pattern of the Subtropical Gyre (for example, near 36° W), proof is still required that it is 'swimming' north.

Overall, it appears that the eddy is neither moving south due to nonlinearity, decay and collapse or ocean currents. Is it possible that by sinking (*ca.* 40 m a^{-1}), the eddy core is stretching a surface water column and compensating for the vertical Ekman velocity (*ca.* 60 m a^{-1}), resulting in little local Sverdrup transport through the eddy? For a coherent eddy with tangential currents that reach the surface, the Ekman currents may be trapped within the water moving with the core and so the familiar arguments of Ekman pumping may not be applicable. If the eddy is resisting the southward flow of the ocean this would imply a frictional drag to the south on the eddy as a whole (balanced by a coriolis force to the north, marginally adding to the westward beta effect).

In the broadest sense of conservation of potential vorticity $(f + \zeta)/H$, the westward movement (f constant) can be viewed as implying changes in thickness (H) and relative vorticity ζ. The core value of $|\zeta|$ appears to have increased (i.e. become more negative), which implies H has decreased which would be expected from decay or collapse of the central structure and this will have to occur in such a way as to steepen the internal structure (see also § 7 *c*). Imagine an idealized situation where two isopycnals contain an eddy core in solid body rotation and that the initial separation thickness is $H_1 = H_0 + h$ in a central region, $r < L$, where the relative vorticity is constant. $H_0 \sim 50$ m is the far field separation and h is the separation anomaly with an initial mean value h_1 to a radius $r = L$. Then, assuming no frictional torque,

$$(f_1 + \zeta_1)/H_1 = (f_2 + \zeta_2)/H_2, \tag{5.2}$$

where the subscripts '1' and '2' refer to the initial and later periods, respectively. Now for the sake of argument, assume that changes over a *ca.* 300 d period were not due to subduction with $f_1 \sim f_2 \sim f$, $\zeta_1/f = -0.3$, $\zeta_2/f = -0.4$, $h_1 \sim 90$ m, then these values give a mean collapse of $H_2/H_1 \sim 86\%$ (*ca.* 83% if account is taken for the small change in latitude one degree to the south) over the period with $h_2 = 70$ m. The central structure will be steeper than before as the core is rotating faster.

6. Eddy origin

It is just possible that the eddy formed in the region where it was first observed at the end of April near *ca.* 25° W, but the sea surface temperature was already 20.6 °C when the buoy was at this position. Intense local vertical mixing (but not below *ca.* 150 m, or below about 19 °C) might have resulted in a local formation.

Extrapolating the eddy movement (see figure 1) might suggest that the eddy originated south of the Canary Islands, or even near West Africa with eddy shedding on the continental slopes. However, the salinity core characteristic of 37.06 psu (table 1)

PHILOSOPHICAL TRANSACTIONS OF THE ROYAL SOCIETY A MATHEMATICAL, PHYSICAL & ENGINEERING SCIENCES

precludes a formation east of about *ca.* 20° W (CTD 3; see figure 4). The core water at *ca.* 200 m is likely to have come from nearer the sea surface, as maximum mean salinities in the Subtropical Gyre do not exceed *ca.* 36.8 psu at a depth of 200 m in the North Atlantic. The required temperature characteristic (*ca.* 20 °C), at the salinity of 37.06 psu, probably means a surface winter formation followed by subduction. The Argos buoys have measured surface temperature in the region covering three winters (figure 23). Calibrated surface (0.5 m) winter temperatures (19.2 °C) in the vicinity of Great Meteor Tablemount were measured by buoy 3346 in the winter of 1992/1993. Winter temperatures of 19.9 °C, at a more southerly position near 26° N, 22° W, were found in early 1993, and this region could be the formation area (where buoy 3346 may have had its first encounter with the eddy near yearday 48, table 3). These temperatures (*ca.* 19.9 °C) also occurred locally in the surrounding waters, persisting until yearday *ca.* 85. It is possible that the eddy formed near this location (or just slightly north *ca.* 1 or 2°) in January 1993. The characteristic salinity and temperature core values also exist to the north (at *ca.* 28° N) and stretch west (to about *ca.* 30° W) in late winter (Levitus 1982) but it is unlikely that the eddy formed along this region the previous winter (figure 24). Formation west of 25° W is not consistent with the general westward movement for this eddy; there do not appear to be strong currents necessary to sweep the eddy first eastward, though southward flow occurs west of the Canary Islands (to *ca.* 22 W). Indeed, buoy 3346 came south from a position near *ca.* 30° N, 22° W in this eastern boundary flow of the Subtropical Gyre in November, December 1992 and January 1993 at a mean southward speed of 5 cm s^{-1} (a value representing conditions at a depth of 200 m, the drogue depth).

A winter formation means the eddy core was exposed at the sea surface and initially under the influence of air–sea interaction (i.e. heat and salt (fresh water) fluxes). Further speculation might include how the core properties changed as the seasonal thermocline developed in 1993. Some warming of the upper core would have taken place as the seasonal thermocline developed. Although the thermocline may later act as an insulator, it will probably be at a cost to the size of the original eddy or amount of water originally comprising the eddy. Ultimately, the differing densities between the water below and above the developing thermocline will result in separate evolution paths for these two contrasting bodies of water even though the core below may be able to carry the thermocline and wind mixed layer for considerable distances. Mixing along isopycnals in the region of relatively large density difference between the top of the core and the base of the thermocline might also allow some contrasting salinity perturbations in this region capable of modifying the upper core. Small-scale density-compensating salinity structure was observed in some CTD profiles.

By the winter of 1993/94, the subducting eddy had buried itself sufficiently within the surface waters of the Subtropical Gyre to escape any further exposure to the atmosphere, with sea-surface temperatures not falling below *ca.* 21.2 °C, leaving a cap of warm water (*ca.* 1.3 °C temperature difference) covering the eddy core in January, February and March 1994 (figure 23). However, as the thermocline was eroded and the wind mixed layer deepened, some enhanced mixing of the upper eddy core properties might be expected.

Temperature, salinity and oxygen eddy core characteristics are consistent with a winter formation. Overall, the measured winter sea surface values of temperature (1992–1994) and salinity were in good agreement with the historical data and these water mass properties coupled with the constant westward moving tendency of the eddy indicate that Swesty was formed near the eastern boundary of the Subtropical

PHILOSOPHICAL TRANSACTIONS OF THE ROYAL SOCIETY A MATHEMATICAL, PHYSICAL & ENGINEERING SCIENCES

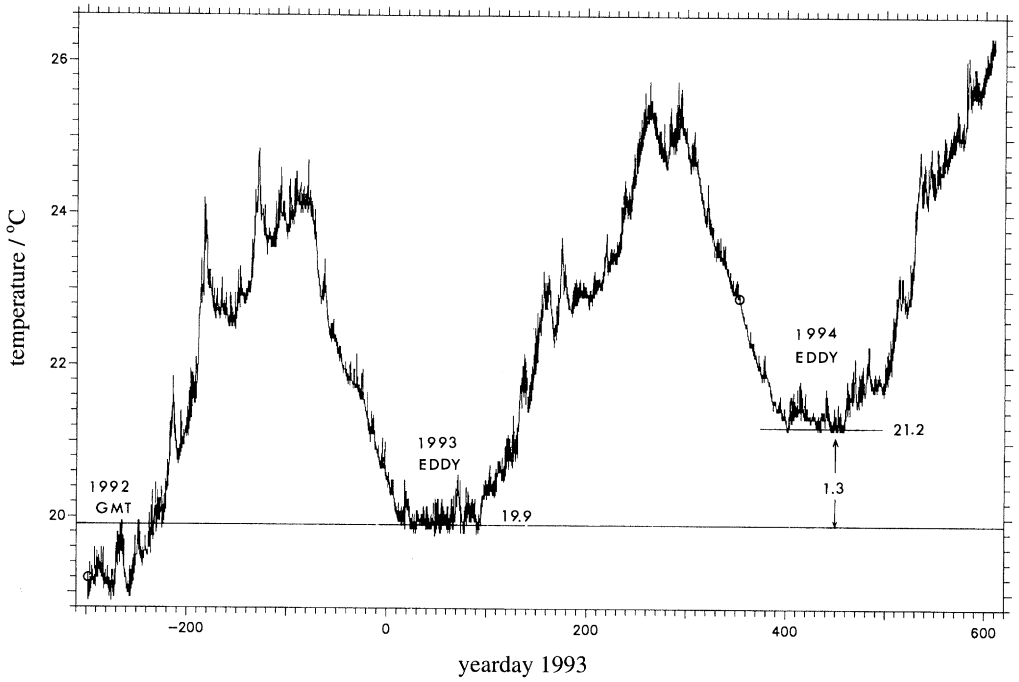

Figure 23. Surface (0.5 m) temperatures in the eastern Subtropical Gyre against yearday 1993 (i.e. from March 1992 to September 1994) measured by the drogued buoys. Winter temperatures in 1992 represent conditions near Great Meteor Tablemount (GMT), measured by buoy 3346. Winter minimum temperatures in 1994 were measured by buoys in the eddy. The 1993 winter temperature minimum was 19.9 °C, the core value of the eddy. Buoy 3346 was in the eddy continuously from yearday 115–356 and buoy 3915 continued measuring surface temperature to yearday *ca.* 620. Two circles are temperature calibration checks (within *ca.* 0.05 °C of the measured values) made on deployment and recovery.

Gyre in the vicinity of *ca.* 26–27° N, 21–23° W in January or February 1993. The eddy was therefore a 'one year old' in the winter of 1993/94 just after the hydrographic survey and already a subducted water parcel which would be expected to sink further. Whether Swesty formation results from flow instability near the eastern boundary or from winter mixing, providing a core of mode water properties, is still unknown. If the Eastern Boundary is important in the generation process, then other Swesties might be generated near 20° W from, say, 24° N to as far north as the subtropical front or Azores current *ca.* 34° N, a region covering *ca.* 1000 km.

7. Order of magnitude estimates for effective mixing coefficients

Some anticyclonic eddies (e.g. Meddies) have a marked water mass core (a salinity anomaly of *ca.* 1 psu) and are important in the transfer of heat and salt thousands of kilometres through the ocean. Exterior to the water mass front containing the core properties is a region of intrusive interleaving and the rate of advance of this region towards the eddy centre has been used to derive estimates of vertical and horizontal eddy diffusion due to thermohaline intrusions (Ruddick & Hebert 1988). The Swesty has an anomaly (along an isopycnal surface to a radius of *ca.* 60 km) of only 0.06 psu (see also figure 6), though this value would be expected to increase

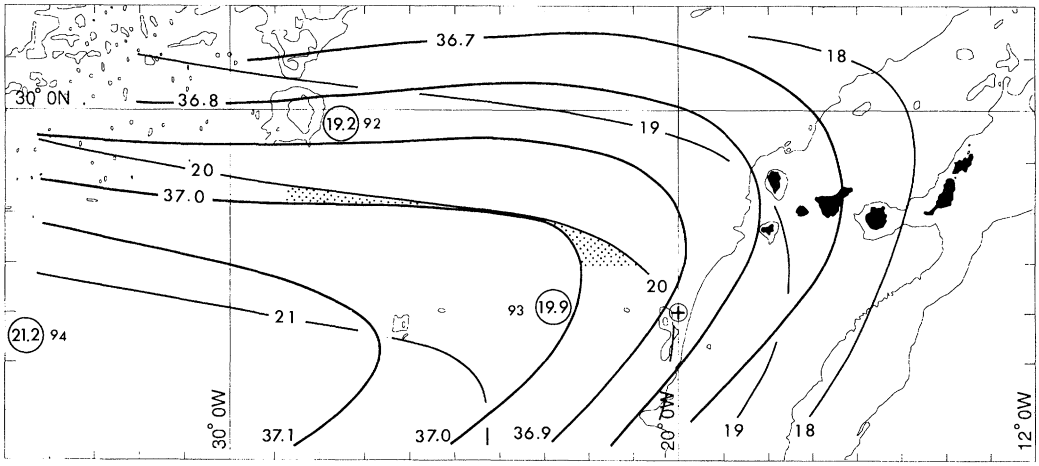

Figure 24. Winter (February March April) surface (50 m) contours of temperature (°C) and salinity (psu) covering the eastern portion of the eddy track (see figure 1). Values in circles are winter minimum temperatures in 1992, 1993 and 1994 measured by the drogued buoys. Cross is position of CTD 3, where the December 1993 surface salinity was 37.07 psu. Stippled region between the 20 °C and 37.0 psu contours indicates the surface region where the winter temperature and salinity values approach the core properties of Swesty.

(in the absence of mixing) as the eddy tracks westward. These eddies are therefore unlikely to play an important role in the transfer of heat and salt and other methods need to be found to derive effective mixing coefficients. Despite mixing and dilution of core water along isopycnal surfaces, a discrete parcel of water largely representing the original water is believed to have travelled with the eddy, otherwise the buoys would not have remained in the eddy for such extended periods. Unless buoys are very carefully drogued, they do not remain in eddies (*ca.* 50 km radius) in windy conditions for any length of time (greater than 20 d, say).

Without a distinctive central water mass, effective diffusion coefficients cannot be derived from the hydrographic structure near the core but may be instead broadly estimated from the decay of the kinematic structure. The eddy has probably survived for *ca.* 19 months (*ca.* 600 d), if formed by winter mixing near 22° W. Assume on the basis of the present results (e.g. tangential velocity just exterior to the central core, figure 20) that the half-life of the eddy is about *ca.* 300 d. Here, the half-life is defined broadly as the time taken for an average core anomaly property (e.g. Brunt–Vaisala frequency, figure 10) to fall by diffusive processes to half its initial anomaly. Some properties may be increasing locally as a result of dynamic processes (e.g. potential vorticity, figure 21), nevertheless diffusion will continue to operate overall acting to decay or reduce the size of the anomaly structure.

(*a*) *Vertical mixing*

First, assume only vertical mixing and a cosine anomaly (i.e. $\cos(\pi z/2l)$. Then by analogy with linear heat flow in a slab (Carslaw & Jaeger 1959), the time t taken for the anomaly of thickness $2l$ to fall to 50% of its initial value is

$$K_{\mathrm{v}}\pi^2 t/4l^2 = 0.69, \tag{7.1}$$

and with $2l \sim 100$ m (an average vertical scale), $K_{\mathrm{v}} \sim 0.3\ \mathrm{cm^2\ s^{-1}}$, comparable to that ($0.3\ \mathrm{cm^2\ s^{-1}}$ for salt) determined by Ruddick & Hebert (1988) for Meddy

Sharon, due to interleaving processes alone. The value of K_v is, as expected, larger than $K_v \sim 0.15\ \mathrm{cm^2\ s^{-1}}$, recently determined by Ledwell *et al.* (1993) from an open ocean tracer release experiment for the upper permanent thermocline in this region since all the decay has been assumed to result from vertical mixing. Relatively larger values would be expected in the regions of increased vertical shear, particularly at a radius of 30 km near a depth of 300 m. It is noted that the eddy actually passed through the position (but later) of this open ocean tracer release site (tracers will also be important in establishing the long-term mean flow, see § 5). Low values are to be expected in this near-surface region since the mean kinetic energy is particularly low (*ca.* $30\ \mathrm{cm^2\ s^{-2}}$, see § 8; cf. Rockall Trough *ca.* $300\ \mathrm{cm^2\ s^{-2}}$, Pingree 1993).

(*b*) *Horizontal mixing*

Now assume that only horizontal mixing is effective and then, treating the initial anomaly as uniform and contained within a circular cylinder of diameter $2l$, the time t for the average value to fall $\times 0.5$ is given (Carslaw & Jaeger 1959) by

$$K_h t/l^2 \sim 0.06. \tag{7.2}$$

With $l \sim 40$ km (mean horizontal scale, giving aspect ratio *ca.* 0.1%, see, for example, figure 10), $K_h \sim 4 \times 10^4\ \mathrm{cm^2\ s^{-1}}$. This value is small compared with oceanic estimates of horizontal diffusion *ca.* $10^8\ \mathrm{cm^2\ s^{-1}}$ (Okubo 1971), but comparable with an estimate (*ca.* $2 \times 10^4\ \mathrm{cm^2\ s^{-1}}$) based on particle separation in a coherent vortex structure (Pingree & le Cann 1992*b*). Schultz Tokos & Rossby (1991) found a value of K_h (for salt) *ca.* $3 \times 10^4\ \mathrm{cm^2\ s^{-1}}$ for meddy Sharon. The overall consistency with other diffusion values suggests that 300 d is a reasonable estimate for the eddy half-life.

(*c*) *Temperature perturbation structure*

Although diffusion rates were not estimated from the temperature gradient structure, the small-scale structure of temperature was derived in the manner of Pingree & Le Cann (1993*a*) in order to appraise the eddy density perturbation structure and to derive a cross section of small-scale temperature structure. Each individual Sea-Soar profile was smoothed with a running mean of 10 m and then subtracted from the actual profile. A 135 km section to 400 dbar of 70 profiles (from C to D, figures 3 and 8) is illustrated in figure 25. The wind-mixed layer is, as expected, homogeneous or without structure. The large perturbation region at *ca.* 110 m depth is simply a manifestation of the seasonal thermocline, which is a large vertical perturbation on the 10 m scale, and not the eddy signature we are looking for, except its upward doming. The eddy core is, as expected, a quiet region. Perturbations increase below a homogeneous core, where vertical temperature gradients also increase (figure 5). The general region, where the perturbations increase around a quiet core, although somewhat ill-defined, has the largest aspect ratio (*ca.* 0.2%) yet determined from the measured eddy properties and might perhaps suggest additional perturbation structure eroding the eddy laterally. Preferential erosion of the eddy at the edges where the lateral shear or strain (4.4) is large could sharpen (by entrainment processes) horizontal density gradient structure (i.e. fronts). Near the core, the lack of vertical shear and the tendency for near-solid-body rotation (characteristics of flow where rotation is important) will inhibit turbulent transfer to smaller scales (and decrease associated diffusive fluxes) thereby insulating the hydrographic properties of the inner core. Increases of horizontal density gradient acting to steepen the isopycnals

PHILOSOPHICAL TRANSACTIONS OF THE ROYAL SOCIETY A MATHEMATICAL, PHYSICAL & ENGINEERING SCIENCES

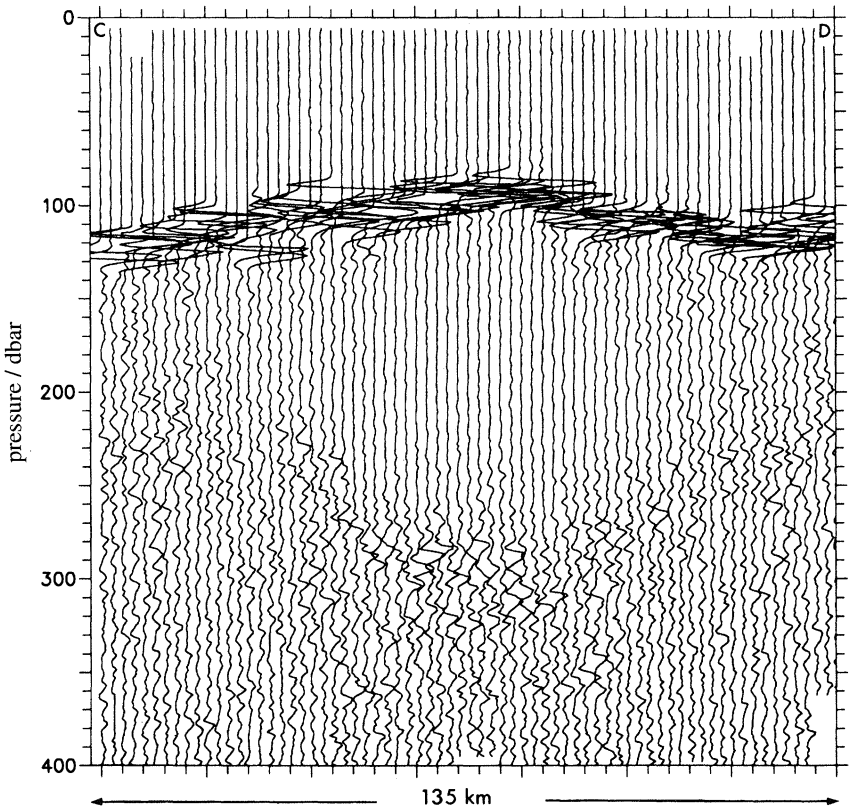

Figure 25. Seventy temperature perturbation profiles through the eddy core from C to D (figures 3 and 8). The section is 135 km across and each profile is displaced by a scale of 0.1 °C. Mixed layer and eddy core are conspicuous by the absence of small-scale structure.

near the central structure could (with geostrophic adjustment) perhaps contribute to the inner region rotating faster with time, as the eddy is eroded away from its outside.

Overall, however, since the perturbation structure tends to reflect vertical temperature (density) gradients, it will tend to match the Brunt–Vaisala frequency distribution (figure 10), and the perturbation minimum (i.e. absence of structure) is centred near a pressure of 190 dbar. The Brunt–Vaisala frequency distribution also tends to have a slightly larger aspect ratio within the central region (see figure 10). However, there is one important difference between figures 10 and 25. The absence of perturbation structure in the eddy core extends to the base of the seasonal thermocline, whereas values of N have increased four fold in this region over their minimum values (*ca.* 1 cph). The increase in N may reflect some initial warming of the upper core as the thermocline was established. The absence of structure in this region suggests that the top of the eddy core is not being actively mixed from above. The thermocline is tending to act as an insulator (but perhaps with a central leak), resulting in preferential erosion of the core along its flanks and from below. At, say, $N = 3$ cph, there is more small-scale structure both below the core and at the sides than above. Salinity fluctuations (not shown) were similarly distributed. A separation of salinity fluctuations along the mean local T–S gradient (i.e. along the slope of the T–S curve) reflecting vertical mixing and internal waves and along the direction of the

local constant isopycnal (i.e. fluctuations along isopycnal lines on the T–S curve) reflecting isopycnal exchanges did not show significant differences in the distributions of these two properties.

8. Eddy kinetic energy and variance

Position fixes (averaging 7.1 values a day) were interpolated to 3 h positions and velocity components at 12 h intervals were derived from mean positions over 12 h to reduce position fixing noise (see figure 17). The resulting mean kinetic energy of all buoys in the eddy was 73 $cm^2\ s^{-2}$ (includes the mean); the maximum speed achieved by a buoy over a 24 h interval for the whole two buoy-years of eddy data was only 30 $cm\ s^{-1}$ (table 3). The eddy was nevertheless energetic in comparison to external conditions, which showed a kinetic energy of 29 $cm^2\ s^{-2}$ (which also includes the mean flow *ca.* 4 $cm\ s^{-1}$, a *ca.* 30% contribution) and a maximum current speed (over a day) of 14 $cm\ s^{-1}$ (table 4) over a period of nearly one year. The low background kinetic energy levels extend for large distances and a kinetic energy of *ca.* 32 $cm^2\ s^{-2}$ was derived from the movement of buoy 3346 during the first year of its travel from the Great Meteor Tablemount to the eddy origin position (figure 1). The low background levels of kinetic energy at a depth of 200 m are also thought to have played a role (an inactive one) in the long survival of this relatively small eddy of low aspect ratio. The variance from the mean of the east component of velocity was 70 $cm^2\ s^{-2}$ for the buoys in the eddy; the north–south variance was *ca.* 66 $cm^2\ s^{-2}$. These values include about a 5% contribution from inertial motion (see § 9) so the mean eddy RMS velocity (to a radius of about 60 km) at the level (*ca.* 200 m) near the maximum current level (*ca.* 175 m) is particularly low *ca.* 11 $cm\ s^{-1}$ (see also figure 20). The area mean of (4.6) to a radius $r = 60\ km \sim Ro\sqrt{2}$ (i.e. water carried along by the eddy at a depth of 200 m) is 12 $cm\ s^{-1}$; the kinetic energy mean of (4.6) at the same level is *ca.* 80 $cm^2\ s^{-2}$. If to this energy we add a mean and an inertial contribution then the total kinetic energy at the core depth for the central period is three times the background level.

9. Energy spectrum and filtered eddy and inertial components

All buoy position values were averaged over 4 h intervals and interpolated to positions at exactly 4 h increments; subtraction gave a velocity time series for each buoy with a value every 4 h. A mean kinetic energy density spectrum was derived from five 100 d length records (buoy, yearday 1993; 3346, 120–220; 1811, 356–456; 3919, 356–456; 3915, 356–456 456–556) for periods when the motion of a buoy was near (*ca.* < 50 km) the eddy centre; a low frequency eddy band, an inertial band and tidal spectral lines are clearly evident (figure 26). The low-frequency eddy band has its peak near 0.004 cph (10.4 d period). There is perhaps a shoulder near the 'harmonic' at 0.008 cph. The inertial spectral band (1/inertial period $\sim$ 0.036 cph at 25.5° N) is separated from the eddy band. The inertial band spreads towards the red end of the spectrum beyond the cut-off at f as the inertial waves in the eddy also feel the influence of the negative relative vorticity of the eddy motion, effectively reducing f (Mooers 1975; Weller 1982; Kunze 1985), though this effect was less marked than has been noted in other situations, where the buoy remained in a region of higher relative vorticity (Pingree 1994). Spectral lines at K_1, M_2, S_2 frequencies have values that are conspicuously elevated above a low background noise level (some of which is

PHILOSOPHICAL TRANSACTIONS OF THE ROYAL SOCIETY A MATHEMATICAL, PHYSICAL & ENGINEERING SCIENCES

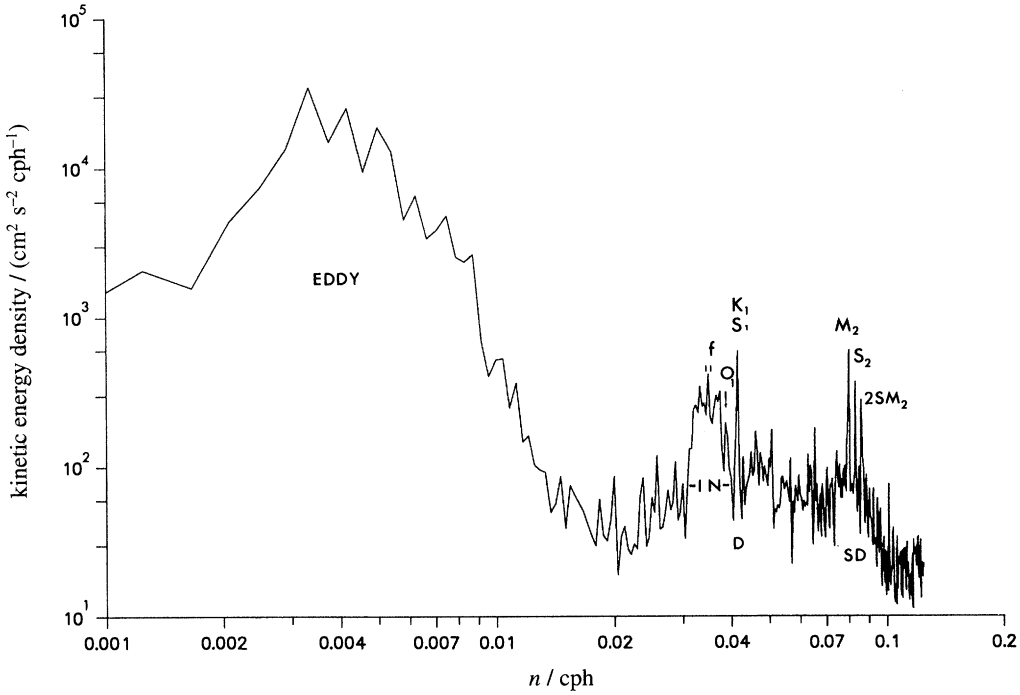

Figure 26. Spectrum of kinetic energy density against frequency n in cph of five 100 d velocity records from drogued buoys in the eddy (see text for details) showing eddy energy. An inertial band (IN) of energy is evident centred about the inertial frequency f. The width of the mark below f shows the range of f from 24.5–25.5° N. Diurnal peaks are marked near D and semidiurnal peaks near SD.

white noise due to position fixing error). Since there are five values for each spectral estimate, significance occurs if a spectral value is elevated above the local variance near the estimate. It is not clear why the K_1 (or S_1) is so marked with respect to the O_1, and this component is probably radiational rather than tidal. The spectra of the five individual 100 d records were not markedly different except in the low-frequency eddy region when a buoy assumed a larger or smaller orbit; one section (3915, 456–556) did not show the marked diurnal peak. An unknown 10 h component was sometimes evident. The individual records were split into clockwise and anticlockwise components (Gonella 1972) and between 93% and 96% of the total energy (i.e. sum of clockwise and anticlockwise energy) in a record was contained within the clockwise components.

Figure 27 gives the clockwise components of the Fourier series that make up the clockwise motion of drogued buoy 3915. The clockwise and anticlockwise Fourier components can be used to filter the high-frequency components from the buoy velocity record (see figure 17) to reveal the eddy orbital motion and extract the inertial signal. Running means cannot be used to remove the high-frequency noise from circular motion without attenuating the amplitude of circular motion at the same time. Subsurface floats with only *ca.* 2 fixes a day cannot readily resolve inertial and semidiurnal tidal motion and these motions would be aliased in the spectral estimates.

With such obvious spectral gaps (figure 27), it is a relatively simple matter to filter out the eddy motion and the inertial motion. All the records were treated in the same

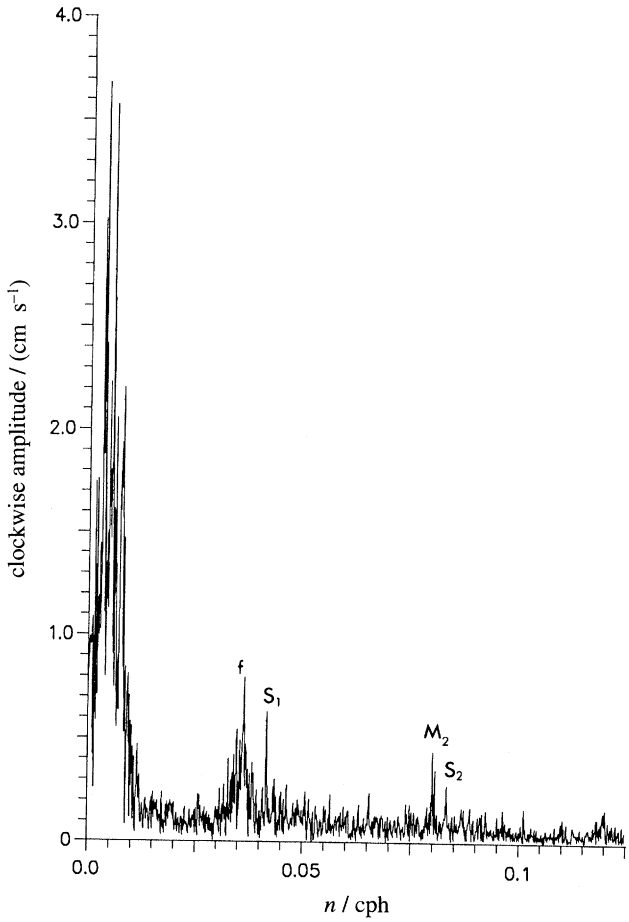

Figure 27. Clockwise component of velocity of buoy 3915 (296 d record) against frequency n in cph showing eddy rotation frequency band and an inertial band together with tidal lines at S_1, M_2 and S_2 frequencies. 'f' is placed at the inertial frequency for 25° N.

manner and an eddy band (2–60 d) and an inertial band (*ca.* 1–2 d) were extracted in the frequency domain. The kinetic energy of the eddy band was 65 cm^2 s^{-2}; the inertial band contained 5% of the energy in the eddy band. A reconstituted inertial record is shown in figure 18*b*. The inertial motions vary on a time scale of order 10 d; there was no local wind record to examine whether the inertial motions were wind or eddy forced.

The inertial motions experienced by buoy 3915 increased markedly near yearday 620 and it most likely that the drogue became detached at this point. The drogue sensor registered drogue attachment (i.e. a generally vertical buoy attitude with drogue–weight attachment) but the sensor was probably sticking near the vertical position. The increased levels of inertial motion are consistent with the buoy now moving freely in the wind-mixed layer and the drogue acceleration test of Pingree (1993), which effectively filters for the energy band entering through the ocean surface (which inertial waves are an important component), also indicated drogue loss on yearday 620. The probably undrogued buoy appeared to loop partially clockwise,

perhaps under eddy near-surface influence for about a further 10 d before moving off northwestward.

It was indeed unfortunate that buoy 3915 lost its drogue after only 267 d. Buoy 1811 lost its drogue after 300 d but buoy 3919 was still effectively drogued 741 d after deployment (same drogue tests). As already mentioned (see § 1), buoy 3346 had been recovered with its drogue intact after 655 d at sea. The mean time for drogue attachment from an earlier release of eight drogued buoys was greater than 532 d, comparable with buoy transmission times. This value is larger than the value of 452 d given by Pingree (1994), as two of those eight buoys have since been recovered with drogues still attached and effective. Drogue loss ought not to be the limiting factor in tracking a discrete body of water.

The east–west variance in the eddy band (*ca.* 2–60 d) was 66 $cm^2\ s^{-2}$ and the north–south variance 64 $cm^2\ s^{-2}$ with a ratio of about 1.03, similar to the unfiltered estimate. A rotation of axes gave a maximum variance aligned *ca.* 120–300°T, which is in the same quadrant as indicated from the hydrographic survey (figure 14), but the ellipticity there was thought to result from the tilt of the isotherms due to westward flow in the eddy relative to background. It is noted that orbital paths do not necessarily have to have the same paths as the eddy structure (e.g. Kirchhoff vortex; Lamb 1932). The maximum variance (aligned *ca.* 120–300°T) was 67 $cm^2\ s^{-2}$ and 7% larger (in variance) than at right angles (i.e. along *ca.* 30–210°T). Overall, the results are suggestive of a slightly elliptical structure, but it was not possible to determine whether there were significant oscillations about the mean (Kida 1981); the central period appeared orientated more north–south and some of these aspects are perhaps just about discernible in figure 19.

The filtered eddy (buoy) velocities for the data of figure 17 are shown in figure 28 and represent two buoy-years in the eddy (nearly 70 orbits) with the mean removed. The buoy velocities, a representation of the true eddy orbital velocities, appear (as a first approximation) circular overall.

10. Conclusions and summary

A shallow subtropical westward propagating eddy (Swesty) has been followed by drogued Argos buoys across the eastern basin of the North Atlantic Ocean from a longitude of *ca.* 25° W to a longitude of *ca.* 41° W near the latitude of 25° N. The eddy was first clearly apparent near *ca.* 25° W and moved at a westward speed of 100 km $month^{-1}$ across the eastern basin towards the Mid-Atlantic Ridge. A hydrographic survey of the eddy was made from RRS Charles Darwin in December 1993 near 33° W. The survey showed that the eddy had a diameter of about 100 km with a core at a depth of 190 m, which was about 150 m thick at the centre. The core appeared slightly tilted and its centre was associated with a small (0.25 °C) sea surface cooling. The eddy core, a time capsule for temperature and salinity, was enclosed within a region of high stability (Brunt–Vaisala frequency *ca.* 3.5 cph) and was characterized by a temperature of 19.9 °C and salinity 37.06 psu, but at this position these properties were close to background values and therefore the eddy core was not very conspicuous on a T–S plot. The tilt of the deeper isotherms (400 m level) was interpreted as revealing the westward movement of the eddy and consistent with the elliptical depth contours of the deeper isotherms. Vertical gradient (Brunt–Vaisala frequency, perturbation structure) and dynamic properties (potential vorticity) revealed the eddy structure well. The small-scale vertical structure of temperature profiles revealed the eddy core and the absence of perturbations extended

PHILOSOPHICAL TRANSACTIONS OF THE ROYAL SOCIETY A MATHEMATICAL, PHYSICAL & ENGINEERING SCIENCES

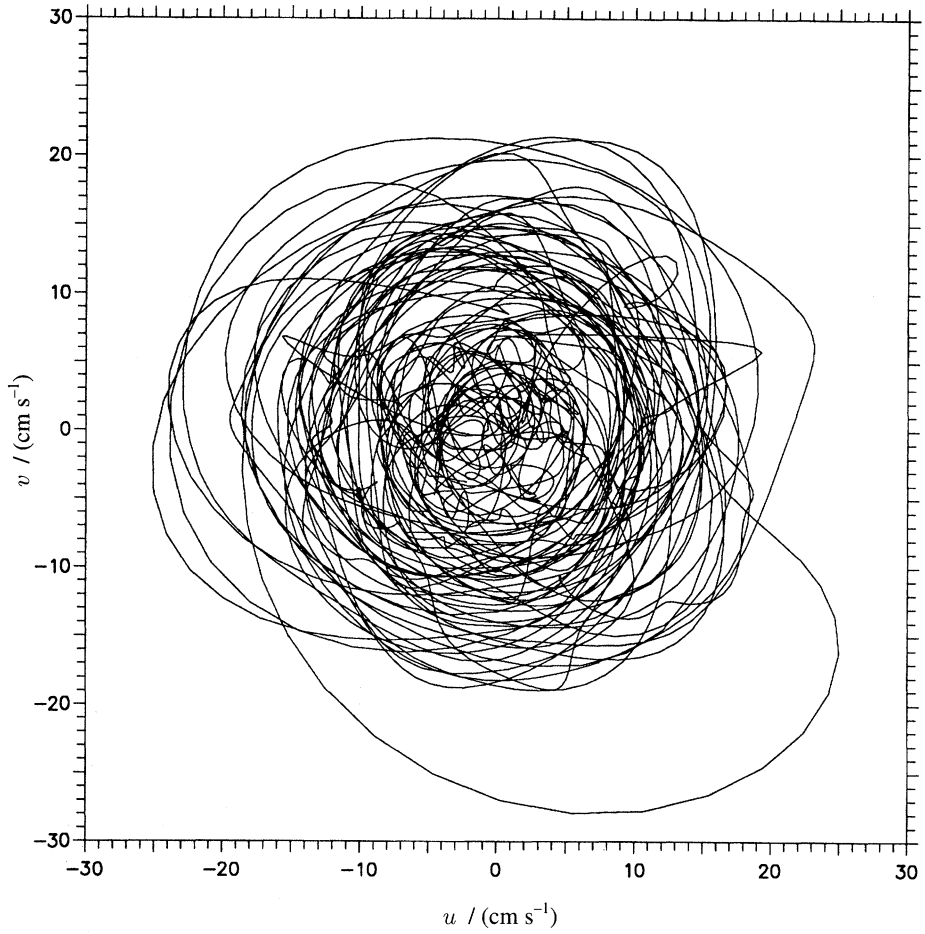

Figure 28. North component of velocity, v, plotted against east component, u, showing the orbital velocity of the eddy motion experienced by the drogued buoys, representing about two buoy-years in the eddy. The data has been filtered in the frequency domain to remove inertial, tidal and very low-frequency components and represents the motion with period of *ca.* 2 d to 60 d.

upwards to the base of the seasonal thermocline. The eddy structure was particularly flat (with respect to other surveyed eddies, table 2) with an aspect ratio of only *ca.* 0.14% (using Brunt–Vaisala distribution) and a vertical decay scale of *ca.* 250 m was estimated for the isotherm displacements below the eddy core. The eddy azimuthal transport was correspondingly small *ca.* 3 Sv. Despite its relatively small size, the potential vorticity was 1.5×10^{-11} rad ms^{-1} in the centre of the core, an order of magnitude lower than background, guaranteeing continued further survival. Three further Argos buoys, drogued at a depth of 200 m, were deployed and the original buoy, which had been at sea for 655 d, was recovered, complete with drogue. Two of the buoys remained in the eddy for a further four months; buoy 3915 looped a further *ca.* 800 km westward.

Overall, there were about two years of buoy data in the eddy, and the eddy was followed continuously for *ca.* 500 d. Maximum azimuthal currents were only *ca.* 16 cm s^{-1} at a radius of 30 km. While the outer region of the eddy appeared to

be slowing as the eddy diminished in size, the central rotation rate appeared to increase over the study period. Rotation periods of *ca.* 8 d in June 1993 and *ca.* 5 d in August 1994, suggested an increase in the magnitude of the central normalized relative vorticity of *ca.* 0.3–0.5 (table 3). However, this increase in central rotation rate could be partly interpreted as evidence for subduction. Bounds were put on effective horizontal and vertical mixing coefficients using an eddy half-life of *ca.* 300 d. The average kinetic energy level for buoys in the eddy was 73 $cm^2\ s^{-2}$; values external to the eddy were particularly low, 29 $cm^2\ s^{-2}$ (table 4). The mean kinetic energy level for the water moving with the eddy core at a depth near *ca.* 200 m was *ca.* 3 times background levels for the central observation period. The variance from the mean for the east–west velocity component of the buoys in the eddy was about 5% larger than the north–south value with maximum variance aligned 120–300°T. A spectral analysis of the buoy's motions showed separate eddy, inertial and tidal energy bands and the results were used to filter the inertial and eddy motions and to determine the point at which buoy 3915 lost its drogue.

The characteristic properties of temperature (19.9 °C), salinity (37.06 psu) and oxygen (4.8 $ml\ l^{-1}$) encapsulated in the eddy core indicated a winter generation near the eastern boundary of the Subtropical Gyre near *ca.* 27° N, 22° W. Although getting smaller, the eddy was almost able to maintain its latitude moving at a near constant westward speed (*ca.* 3.7 $cm\ s^{-1}$) while under the influence of the southward flow of the Subtropical Gyre, slipping only about one degree south over the continuously drogued observed *ca.* 1650 km journey. The straightness of its track suggests that the eddy was able to resist local current variability. Part of the eddy's observed travel distance is the result of westward advection. When the flow of the Subtropical Gyre is taken into account, the westward propagation speed is reduced from 3.7 $cm\ s^{-1}$ to 2.2 $cm\ s^{-1}$. This value seems rather large for the beta effect (in comparison with other eddies and a theoretical estimate). The apparent increase in the magnitude of the relative vorticity of the central region (coupled with vertical squashing) may have helped the eddy to maintain its latitude.

Hydrographic measurements conducted on the outward route to the eddy survey region revealed isopycnals sloping downward to the west. The core isopycnal ($\sigma_0 = 26.37\ kg\ m^{-3}$) and historical data showed that the eddy must be sinking or subducting at a rate of about 40 m a year. Original water markedly modified by the development of the seasonal thermocline would be expected to follow a different route. Winter surface temperatures (measured by the three drogued Argos buoys in the eddy) in 1993/1994 did not fall below 21 °C and no further air–sea exchange or loss of core properties took place on Swesty's first birthwinter.

It is not known if Swesty production is a rare phenomenon or even how many Swesties there are in the subtropical North Atlantic Ocean at a given time. No further surface eddies were found on the 1500 km route to the eddy survey area. The absence of a distinctive core and the thinness of the density anomaly (maximum target *ca.* 150 m, for a central strike with an exploratory XBT drop) make these eddies relatively difficult to detect. This may partly account for the delayed discovery of this type (anticyclonic, with a core of original water properties) of surface subtropical eddy, subducting westward through the World's much studied gyre.

Bob Head (PML) kindly performed the nutrient analyses and Pablo Serret (University of Oviedo, Spain) the oxygen concentrations. The SeaSoar was borrowed from IOSDL. Ron Easton (PML) constructed the drogues at sea; Dr Bablu Sinha assisted with the data processing and analysis. Part of this study has been carried out with the support of U.K. WOCE funding and the Procurement Executive, Ministry of Defence.

References

Angel, M. V. & Fasham, M. J. R. 1983 Eddies and biological processes. In *Eddies in marine science* (ed. A. R. Robinson), pp. 493–524. Berlin: Springer.

Armi, L., Hebert, D., Oakey, N., Price, J., Richardson, P., Rossby, T. & Ruddick, B. 1989 Two years in the life of a Mediterranean salt lens. *J. Phys. Oceanogr.* **19**, 354–370.

Armi, L. & Stommel, H. 1983 Four views of a portion of the North Atlantic Subtropical Gyre. *J. Phys. Oceanogr.* **13**, 828–857.

Carslaw, H. S. & Jaeger, J. C. 1959 *Conduction of heat in solids*, 2nd edn, pp. 510. Oxford University Press.

Colin de Verdiere, A. 1992 On the southward motion of Mediterranean salt lenses. *J. Phys. Oceanogr.* **22**, 413–420.

Cushman-Roisin, B., Chassignet, E. P. & Tang, B. 1990 Westward motion of mesoscale eddies. *J. Phys. Oceanogr.* **20**, 758–768.

Davis, R. E., Webb, D. C., Regier, L. A. & Dufour, J. 1992 The autonomous Lagrangian circulation explorer (ALACE). *J. Atmos. Ocean. Technol.* **9**, 264–285.

Flierl, G. R. 1981 Particle motion in large-amplitude wave fields. *Geophys. Astrophys. Fluid Dyn.* **18**, 39–74.

Gill, A. E. 1982 *Atmosphere–ocean dynamics*, pp. 662. London: Academic.

Gonella, J. 1972 A rotary-component method for analysing meteorological and oceanographic vector time series. *Deep Sea Res.* **19**, 833–846.

Isemer, H. & Hasse, L. 1987 *The Bunker climate atlas of the North Atlantic Ocean*, vol. 1, pp. 218. New York: Springer.

Kerr, R. A. 1981 Small eddies proliferating in the Atlantic. *Science* **213**, 632–634.

Kida, S. 1981 Motion of an elliptic vortex in a uniform shear flow. *J. Phys. Soc. Japan* **50**, 3517–3520.

Kunze, E. 1985 Near-inertial wave propagation in geostrophic shear. *J. Phys. Oceanogr.* **15**, 544–565.

Lamb, H. 1975 *Hydrodynamics*, 6th edn, pp. 738. Cambridge University Press.

Ledwell, J. R., Watson, A. J. & Law, C. S. 1993 Evidence for slow mixing across the pycnocline from an open-ocean tracer-release experiment. *Nature* **364**, 701–703.

Levitus, S. 1982 Climatological atlas of the world ocean. NOAA Professional Paper 13, pp. 173. U.S. Department of Commerce.

McDowell, S. E. & Rossby, H. T. 1978 An intense mesoscale eddy off the Bahamas. *Science* **202**, 1085–1087.

Mooers, C. N. K. 1975 Several effects of a baroclinic current on the cross-stream propagation of inertial-internal waves. *Geophys. Fluid Dyn.* **6**, 245–275.

Narayanan, S. & Lilly, G. R. 1993 On the accuracy of XBT temperature profiles. *Deep Sea Res.* **40**, 2105–2113.

Nof, D. 1981 On the β-induced movement of isolated baroclinic eddies. *J. Phys. Oceanogr.* **11**, 1662–1672.

Okubo, A. 1971 Ocean diffusion diagrams. *Deep Sea Res.* **18**, 789–802.

Olbers, D. J., Wenzel, M. & Willebrand, J. 1985 The inference of North Atlantic circulation patterns From climatological hydrographic Data. *Rev. Geophys.* **23**, 313–356.

Pingree, R. D. 1993 Flow of surface waters to the west of the British Isles and in the Bay of Biscay. *Deep Sea Res.* II **40**, 369–388.

Pingree, R. D. 1994 Winter warming in the Southern Bay of Biscay and Lagrangian eddy kinematics from a deep-drogued Argos buoy. *J. Mar. Biol. Ass. U.K.* **74**, 107–128.

Pingree, R. D. 1995 The droguing of Meddy Pinball and seeding with ALACE floats. *J. Mar. Biol. Ass. U.K.* **75**, 235–252.

Pingree, R. D. & Le Cann, B. 1991 Drifting buoy in the field of flow of two eddies on East Thulean Rise (north-east Atlantic). *J. Geophys. Res.* **96**, 16 759–16 777.

Pingree, R. D. & Le Cann, B. 1992*a* Three anticyclonic Slope Water Oceanic eDDIES (SWODDIES) in the southern Bay of Biscay in 1990. *Deep Sea Res.* **39**, 1147–1175.

PHILOSOPHICAL TRANSACTIONS OF THE ROYAL SOCIETY A MATHEMATICAL, PHYSICAL & ENGINEERING SCIENCES

Pingree, R. D. & Le Cann, B. 1992*b* Anticyclonic Eddy X91 in the Southern Bay of Biscay, May 1991 to February 1992. *J. Geophys. Res.* **97**, 14 353–14 367.

Pingree, R. D. & Le Cann, B. 1993*a* Structure of a Meddy (Bobby 92) southeast of the Azores. *Deep Sea Res.* **40**, 2077–2103.

Pingree, R. D. & Le Cann, B. 1993*b* A shallow MEDDY (a SMEDDY) from the secondary Mediterranean salinity maximum. *J. Geophys. Res.* **98**, 20 169–20 185.

PML Cruise Report 1992 RRS Charles Darwin Cruise 66/92, 4 March–6 April, pp. 85. Plymouth Marine Laboratory.

PML Cruise Report 1994 RRS Charles Darwin Cruise 83/93, 13 December 1993–13 January 1994, pp. 91. Plymouth Marine Laboratory.

Richardson, P. L., Hufford, G. E., Limeburner, R. & Brown, W. S. 1994 North Brazil Current retroflection eddies. *J. Geophys. Res.* **99**, 5081–5093.

Richardson, P. L., Walsh, D., Armi, L., Schröder, M. & Price, J. F. 1989 Tracking three meddies with SOFAR Floats. *J. Phys. Oceanogr.* **19**, 371–383.

Ruddick, B. & Hebert, D. 1988 The mixing of meddy 'Sharon'. In *Small-scale turbulence and mixing in the ocean.* Proc. 19th Int. Liège Colloq. on Ocean Hydrodynamics (ed. J. C. J. Nihoul & B. M. Jamart), pp. 249–262. Amsterdam: Elsevier.

Schultz Tokos, K. L. & Rossby, T. 1991 Kinematic and dynamics of a Mediterranean salt lens. *J. Phys. Oceanogr.* **21**, 879–892.

Stommel, H. 1958 *The Gulf Stream.* Berkeley, CA: University of California Press.

Weller, R. A. 1982 The relation of near-inertial motions observed in the mixed layer during the JASIN (1978) experiment to local wind stress and to the quasi-geostrophic flow field. *J. Phys. Oceanogr.* **12**, 1122–1136.

Received 8 November 1994; accepted 28 February 1995

PHILOSOPHICAL TRANSACTIONS OF THE ROYAL SOCIETY A MATHEMATICAL, PHYSICAL & ENGINEERING SCIENCES